Original Research

Core Ideas

- We present a locally mass-conservative flow, transport, and root–soil interaction model.
- We include a sustainable, flexible research software framework for plant-scale model development.
- This is an improved model concept for fluid dynamic processes, evaporation, root water uptake.

A New Simulation Framework for Soil–Root Interaction, Evaporation, Root Growth, and Solute Transport

Timo Koch,* Katharina Heck, Natalie Schröder, Holger Class, and Rainer Helmig

We have developed a general model concept and a flexible software framework for the description of plant-scale soil–root interaction processes including the essential fluid mechanical processes in the vadose zone. The model was developed in the framework of non-isothermal, multiphase, multicomponent flow and transport in porous media. The software is an extension of the open-source porous media flow and transport simulator DuMu^x to embedded mixed-dimensional coupled schemes. Our coupling concept allows us to describe all processes in a strongly coupled form and adapt the complexity of the governing equations in favor of either accuracy or computational efficiency. We have developed the necessary numerical tools to solve the strongly coupled nonlinear partial differential equation systems that arise with a locally mass conservative numerical scheme even in the context of evolving root architectures. We demonstrate the model concept and its features, discussing a virtual hydraulic lift experiment including evaporation, root tracer uptake on a locally refined grid, the simultaneous simulation of root growth and root water uptake, and an irrigation scenario comparing different models for flow in unsaturated soil. We have analyzed the impact of evaporation from soil on the soil water distribution around a single plant's root system. Moreover, we have shown that locally refined grids around the root system increase computational efficiency while maintaining accuracy. Finally, we demonstrate that the assumptions behind the Richards equation may be violated under certain conditions.

Abbreviations: DUNE, Distributed Unified Numerics Environment; PDE, partial differential equation.

T. Koch, K. Heck, N. Schröder, H. Class, and R. Helmig, Dep. of Hydromechanics and Modelling of Hydrosystems, Univ. of Stuttgart, Pfaffenwaldring 61, 70569 Stuttgart, Germany; N. Schröder, Voith Paper GmbH & Co KG, St. Pöltener Str. 43, 89522 Heidenheim, Germany, and Institute of Bio- and Geosciences: Agrosphere (IBG-3), Forschungszentrum Jülich GmbH, 52425 Jülich, Germany. *Corresponding author (timo.koch@iws.uni-stuttgart.de).

Natural vegetation as well as cultivated crops play an important role in the global water budget, above and below the surface. Therefore understanding transpiration from vegetation is essential and has to be considered in land–atmosphere models used in climatology and hydrology. The interactions of water and plants need to be analyzed on a broad range of temporal and spatial scales (Fatichi et al., 2016), one of them focusing on the interaction of the root system of a single plant with the surrounding soil. Mathematical models and simulation of the relevant processes can help with the fundamental understanding of plants' reactions to their environment, how plant roots contribute to soil water distribution and flow or adapt to drought, or how they are influenced by soil water contamination or salinization (Shani and Ben-Gal, 2005). Although in situ monitoring methods of the physical processes at the soil–root interface are continuously being improved, measurements remain difficult (Zarebanadkouki et al., 2013).

Mathematical models of coupled soil–root systems have been developed to study the transfer processes between the soil and root systems. Such models can also help in analyzing and interpreting measurements and the design of future experimental setups. Challenges include large differences in spatial and temporal scales and the combination of physical, chemical, and biological processes in a single model. Soil–root models range from single root segment models (Roose and Schnepf, 2008) for local soil–root interface studies, crop models used to predict yields (Malézieux et al., 2009), and models with empirical root uptake functions (Somma et al., 1998), to plant-scale models (Javaux et al., 2008) using

an explicit description of the three-dimensional root system and root system growth. Dunbabin et al. (2013) recently compiled a detailed overview of plant-scale models. This kind of model was also the focus of this study.

Plant-scale models include an explicit description of one or more plant root system architectures embedded in the surrounding soil. The root system is usually represented by a network of discrete cylindrical segments, while physical quantities, such as water pressure, are averaged across the cross-section of the cylinder. This simplification of the root system architecture increases the computational efficiency in comparison with a three-dimensional resolution of roots. As a consequence, the mathematical model is reduced to a one-dimensional partial differential equation (PDE) system formulated on a network domain. The root network is geometrically embedded into the three-dimensional soil system, generally using independent, non-matching meshes. The explicit geometrical description of the root system inside the soil allows modeling of transfer processes at the soil–root interface, as well as a natural description of sap and nutrient transport within the root system. The mathematical model is a coupled PDE system involving one- and three-dimensional PDEs. We subsequently refer to such a system as an embedded mixed-dimension system. Formulating the coupling conditions for the coupled PDE systems on two independently meshed domains with different dimensions can be challenging. For the mathematical analysis of similar systems, see D'Angelo and Quarteroni (2008), Köppl and Wohlmuth (2014), and Roose and Schnepf (2008).

Looking at the processes in the unsaturated soil (vadose zone) around a plant's root system, we can identify typical processes of flow and transport of water and nutrients. An overview is given in Fig. 1. In the root system, important processes are root water uptake, xylem flow and transport of minerals, and root growth. In the soil, root water uptake is a driver for water movement. However, there are competing driving forces like gravity, soil water evaporation into the atmosphere, and water precipitation during rainfall events or irrigation.

To formulate mathematical models of those processes, an abstraction of the system is necessary. To this end, the system is described as a porous medium (soil) with embedded hierarchical biological networks (roots, themselves porous media), adjacent to a free flow domain (atmosphere). Each process in Fig. 1 is either localized in a subsystem or describes a process at the interface of subsystems, effectively coupling together subsystem models to an integrated system model.

Many algorithms have been developed to model soil–root interaction and root architecture. We mention here only a selection that features three-dimensional embedded models interacting with the soil (Pagès et al., 2004; Lynch et al., 1997; Leitner et al., 2010; Diggle, 1988; Clausnitzer and Hopmans, 1994; Postma et al., 2017; Schneider et al., 2010). However, these models are either restricted to the Richards or strongly simplified soil flow models, or they lack the description of soil flow and transport completely and are restricted to specific models for the description of xylem flow and water and nutrient uptake (for a review of the capabilities, see Dunbabin et al., 2013). The numerical schemes of the available models are not generally locally mass conservative, which can be an issue if quantification of tracers and root water uptake is of interest. Only one of the models mentioned by Dunbabin et al. (2013) is publicly available under an open-source license. The root system architecture model SimRoot (Lynch et al., 1997) has been recently extended by a hydrology module and is now available under an open-source license (Postma et al., 2017). However, the models describing water and nutrient movement in the soil and evaporation from soil use, as the authors state, "a simplified C++ implementation of the SWMS model," which is restricted to an incompressible Richards model description of soil flow (see Šimůnek et al., 1995). In contrast, we propose a simulation framework with strong emphasis on a consistent and generalized formulation of the fluid mechanical processes. Furthermore, a flexible structure allows the framework to be coupled with established root system architecture models. Such a complex framework is necessary to analyze process interdependencies in more detail, as well as the relevance of a certain process within the overall system setting. The understanding gained from such analysis may motivate improved models for water distribution influenced by vegetation for models and simulations at the field scale.

In this study, we developed a generalized computational framework for modeling such coupled systems in the vadose zone. The coupling between the root and the soil is flexible in the sense that

- models for the subsystems root and soil can easily be exchanged, i.e., computing the soil flow with the Richards equation or a compositional, non-isothermal, two-phase model;

- it is a fully implicit, nonlinear framework using a Newton–Raphson scheme with numerical differentiation, i.e., nonlinear constitutive equations, complex boundary conditions and boundary models, and fluid and material relations can be easily modified, added, or exchanged;
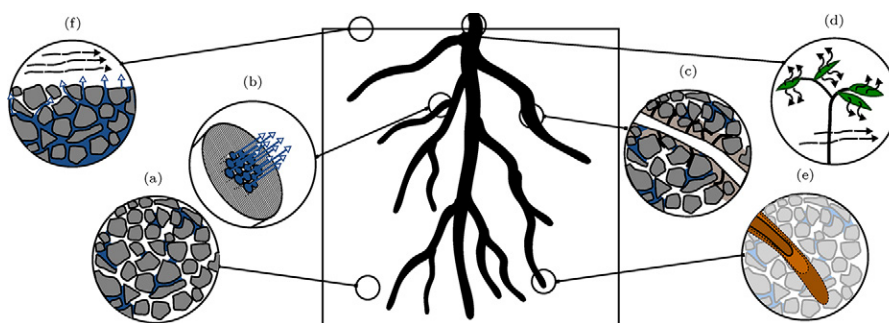

Fig. 1. Typical processes in the vadose zone: (a) flow and transport in unsaturated soil, (b) xylem flow and transport, (c) root water uptake, (d) transpiration, (e) root growth, (f) soil evaporation and water precipitation.

- numerical details and implementation of the coupling conditions are designed independently of the subsystem models, i.e., it is possible to modify the numerical coupling scheme when improved or more efficient versions are available, without changing the models.

The models use locally mass-conservative finite volume schemes in space and implicit Euler in time and are general in that

- equations are only restricted to have a general structure of a conservation equation, $\partial\xi/\partial t + \nabla\cdot f(\xi) = q(\xi)$, with a storage, flux f, and source term q, respectively, for the conserved quantity ξ and t as time;
- constitutive relations in the fluid and material framework are modular and set as properties of the problem;
- grids can be unstructured and locally refined.

The code is available under an open-source license (GNU General Public License). The framework is implemented as an extension to the open-source simulator DuMu$^\text{x}$ (Flemisch et al., 2011) specializing in flow and transport processes in porous media. To our knowledge, there currently exists no framework with these characteristics for plant-scale soil–root interaction modeling in the vadose zone.

Here we present a consistent approach for modeling evaporation from the soil using boundary layer models for the atmosphere and non-isothermal, miscible, two-phase, two-component subsurface flow. The results suggest that evaporation has a significant effect on soil water management, particularly for young plants. We present a coupling scheme modeling root growth and water uptake simultaneously, with improved numerical properties compared with existing growth algorithms concerning mass conservation. We show numerically that we can improve the computational efficiency while preserving accuracy by using soil grids that are locally refined around the embedded root system.

First, we introduce the general concepts for modeling non-isothermal multiphase multicomponent processes in porous media. Second, we refine those concepts for each of the identified fluid mechanical processes. All processes are coupled, resulting in a system of partial differential equations (PDEs) for the multiphysics, mixed-dimension soil–root interaction model. We briefly present the techniques used to solve the model equation systems numerically. We describe the details of the implementation of a generalized numerical framework for such models in DuMu$^\text{x}$. We show four applications realized with the developed model concept, a soil–root model including soil evaporation, a tracer study for root water uptake, a root growth model with simultaneous root water uptake, and an irrigation example. Finally, the presented novelties of the simulation framework are discussed.

Table 1 introduces the symbols used in this paper. Table 2 lists the governing conservation equations necessary to describe the flow and transport processes in the soil and the root system. The constitutive relations used to describe interdependencies between variables can be found in Table 3.

Table 1. List of symbols and abbreviations.

Symbol	Description
α	$\alpha \in \{w, n, s\}$, wetting fluid, non-wetting fluid, solid phase (subscript)
c_s	heat capacity of the solid phase, $J\,K^{-1}$
$D_{\text{eff},\alpha}^{\kappa\vert\pi}$	effective diffusion coefficient of the components κ and π in phase α, $m^2\,s^{-1}$
$D_{\alpha}^{\kappa\vert\pi}$	binary diffusion coefficient of the components κ and π in phase α, $m^2\,s^{-1}$
g	gravitational acceleration, $m\,s^{-2}$
h_α	enthalpy of the fluid phase α, J
κ	$\kappa \in \{H_2O, D_2O, air, ...\}$, water, heavy water, air, etc., components (superscript)
$\mathbf{K}$	intrinsic permeability, m^2
K_{ax}	axial root conductance, $m^4\,s^{-1}\,Pa^{-1}$
K_{rad}	radial root conductance, $m\,s^{-1}\,Pa^{-1}$
$k_{\text{r}\alpha}$	relative permeability of the fluid phase α
λ_{eff}	effective thermal conductivity, $W\,m^{-1}\,K^{-1}$
λ_α	thermal conductivity of phase α, $W\,m^{-1}\,K^{-1}$
Λ_α	mobility of phase α, $Pa^{-1}\,s^{-1}$
M_α, M^κ	average molar mass of phase α, molar mass of component κ, $kg\,mol^{-1}$
$\phi, \phi_{\text{r}}, \phi_{\text{s}}$	porosity of an (unspecified) porous medium, root porosity, soil porosity
p_α	pressure of the fluid phase α, Pa
p_{c}	$p_{\text{c}} = p_{\text{n}} - p_{\text{w}}$, capillary pressure in a two-phase system, Pa
$p_\alpha^{\;\kappa}$	partial pressure of the component κ in the fluid phase α, Pa
$p_{\text{sat}}^{\;\kappa}$	saturation vapor pressure of the component κ, Pa
$p_{\text{w,root}}, p_{\text{w,soil}}$	pressure of the wetting phase (i.e., aqueous phase) in root and soil, Pa
q	volume source term, reaction term, $kg\,s^{-1}\,m^{-3}$
$\hat{q}$	line source term, $kg\,s^{-1}\,m^{-1}$
R	root segment radius, m
$\mathcal{R}$	universal gas constant, $J\,mol^{-1}\,K^{-1}$
$S_\alpha, S_{\alpha\text{e}}, S_{\alpha\text{r}}$	saturation, effective saturation, residual saturation of the fluid phase α
τ	tortuosity of the porous medium
T	temperature, K
u_α	internal energy of the fluid phase α, J
$x_\alpha^{\;\kappa}, X_\alpha^{\;\kappa}$	mole, mass fraction of the component κ in the phase α
μ_α	dynamic viscosity of the fluid phase α, Pa s
ρ_α	density of the fluid phase α, $kg\,m^{-3}$
$\rho_{\text{m},\alpha}$	molar density of the fluid phase α, $mol\,m^{-3}$
ζ	local axial coordinate of the root, m
z	height, $z = 0$ at the soil surface, upward-pointing axis, m

Table 2. Governing equations and primary variables for various soil and root models.

Model	Equations	Eq.	Primary variables	Description
Two-phase, two-component	$\dfrac{\partial}{\partial t}\left(\sum_\alpha \phi S_\alpha \rho_{m,\alpha} x_\alpha^{H_2O}\right) + \nabla \cdot \sum_\alpha \left(\rho_{m,\alpha} x_\alpha^{H_2O} \mathbf{v}_\alpha - \rho_{m,\alpha} D_{eff,\alpha}^{H_2O|air} \nabla x_\alpha^{H_2O}\right) = \sum_\alpha \dfrac{q_\alpha^{H_2O}}{M^{H_2O}}$	[1]	p_w, S_n $\to$ if both phases $p_w, x_n^{H_2O}$ $\to$ if only w phase p_w, x_w^{air} $\to$ if only n phase	soil-water dynamics
	$\dfrac{\partial}{\partial t}\left(\sum_\alpha \phi S_\alpha \rho_{m,\alpha} x_\alpha^{air}\right) + \nabla \cdot \sum_\alpha \left(\rho_{m,\alpha} x_\alpha^{air} \mathbf{v}_\alpha - \rho_{m,\alpha} D_{eff,\alpha}^{H_2O|air} \nabla x_\alpha^{air}\right) = \sum_\alpha \dfrac{q_\alpha^{air}}{M^{air}}$	[2]		
	with $\mathbf{v}_\alpha = -\dfrac{k_{r\alpha}}{\mu_\alpha}\mathbf{K}(\nabla p_\alpha + \rho_\alpha g \nabla z)$ and $\alpha \in \{w, n\}$			
Richards	$\dfrac{\partial(\phi S_w \rho_w)}{\partial t} - \nabla \cdot \left[\rho_w \dfrac{k_{rw}}{\mu_w}\mathbf{K}(\nabla p_w + \rho_w g \nabla z)\right] = q_w$	[3]	p_w	soil-water dynamics
Richards, two-component	$\dfrac{\partial(\phi S_w \rho_{m,w})}{\partial t} - \nabla \cdot \left[\rho_{m,w}\dfrac{k_{rw}}{\mu_w}\mathbf{K}(\nabla p_w + \rho_w g \nabla z)\right] = \dfrac{q_w}{M_w}$ and $\dfrac{\partial(\phi S_w \rho_{m,w} x_w^\kappa)}{\partial t} - \nabla \cdot \left[x_w^\kappa \rho_{m,w}\dfrac{k_{rw}}{\mu_w}\mathbf{K}(\nabla p_w + \rho_w g \nabla z) + \rho_{m,w}D_{eff}^{H_2O|\kappa}\nabla x_w^\kappa\right] = \dfrac{q^\kappa}{M^\kappa}$	[4]	p_w, x_w^κ	soil-water dynamics
Single-phase (one dimensional)	$\dfrac{\partial(\phi\rho_w \pi R^2)}{\partial t} - \dfrac{\partial}{\partial \zeta}\left[\rho_w K_{ax}\left(\dfrac{\partial p_w}{\partial \zeta} + \rho_w g\dfrac{\partial z}{\partial \zeta}\right)\right] = q_w$	[5]	p_w	root xylem flow
Single-phase, two-component (one-dimensional)	$\dfrac{\partial(\phi\rho_{m,w}\pi R^2)}{\partial t} - \dfrac{\partial}{\partial \zeta}\left[\rho_{m,w}K_{ax}\left(\dfrac{\partial p_w}{\partial \zeta} + \rho_w g\dfrac{\partial z}{\partial \zeta}\right)\right] = \dfrac{q_w}{M_w}$ and $\dfrac{\partial(\phi\rho_{m,w}x_w^\kappa \pi R^2)}{\partial t} - \dfrac{\partial}{\partial \zeta}\left[x_w^\kappa \rho_{m,w}K_{ax}\left(\dfrac{\partial p_w}{\partial \zeta} + \rho_w g\dfrac{\partial z}{\partial \zeta}\right) + \rho_{m,w}D_{eff}^{\pi|\kappa}\dfrac{\partial x_w^\kappa}{\partial \zeta}\right] = \dfrac{q^\kappa}{M^\kappa}$	[6]	p_w, x_w^κ	root xylem flow
Non-isothermal	$\dfrac{\partial}{\partial t}\left[\sum_\alpha (\phi\rho_\alpha u_\alpha S_\alpha) + (1-\phi)\rho_s c_s T\right] - \nabla\cdot\left[\sum_\alpha(\rho_\alpha b_\alpha \mathbf{v}_\alpha) + \lambda_{eff}\nabla T\right] = q^b$ with $\mathbf{v}_\alpha = -\dfrac{k_{r\alpha}}{\mu_\alpha}\mathbf{K}(\nabla p_\alpha + \rho_\alpha g \nabla z)$ and $\alpha \in \{w, n\}$	[7]	T	energy transport

Table 3. Constitutive relations and constraints for the partial differential equation systems in Table 2.

Constitutive relation or constraint	Eq.	Notes
$S_w = [1 + (ap_c)^n]^m$ where $p_c = p_n - p_w$, $m = 1 - 1/n$	[8]	van Genuchten (1980); parameters a, m, and n depend on the soil type; used in miscible two-phase, two-component flow, Eq. [1] and [2], and the Richards flow, Eq. [3]
$k_{rw} = \sqrt{S_{we}}\left[1 - \left(1 - S_{we}^{1/m}\right)^m\right]^2$ $k_{rn} = \left(1 - S_{we}\right)^{1/3}\left(1 - S_{we}^{1/m}\right)^{2m}$ where $S_{we} = \dfrac{S_w - S_{wr}}{1 - S_{wr}}$	[9]	Luckner et al. (1989), van Genuchten (1980), Mualem (1976); used in miscible two-phase, two-component flow, Eq. [1] and [2], and the Richards flow, Eq. [3]
$x_n^\kappa = \dfrac{p_n^\kappa}{p_n}$	[10]	mole fraction in gas phase after Dalton's law (ideal gas mixture); used in miscible two-phase, two-component flow, Eq. [1] and [2]
$x_w^\kappa = \dfrac{p_n^\kappa}{p_{sat}^{H_2O}}$, $p_{sat}^\kappa = p_{sat}^\kappa(T)$ for κ as the main component of α	[11]	mole fraction of the main component in the water phase calculated with the saturated vapor pressure (Raoult's law); used in miscible two-phase, two-component flow, Eq. [1] and [2]
$x_w^\kappa = \dfrac{p_n^\kappa}{H_w^\kappa}$, $H_w^\kappa = H_w^\kappa(T)$ for κ as solutes with small mole fractions	[12]	mole fraction of components in the water phase after Henry's law (thermodynamic equilibrium) for solutes with small mole fraction in liquid; used in miscible two-phase, two-component flow, Eq. [1] and [2]
$\sum_\kappa x_\alpha^\kappa = \sum_\kappa X_\alpha^\kappa = 1$	[13]	used in multicomponent models, Eq. [1], [2], [4], and [6]
$S_n + S_w = 1$	[14]	used in miscible two-phase, two-component flow, Eq. [1] and [2], and the Richards flow, Eq. [3]
$\rho_{m,\alpha} = \dfrac{\rho_\alpha}{\sum_i x_i^\kappa M_i}$	[15]	molar density in mol m^{-3}; used in multicomponent models, Eq. [1], [2], [4], and [6]
$D_{eff,\alpha}^\kappa = \phi S_\alpha \tau D_\alpha^{\kappa/\pi}$	[16]	effective diffusion coefficient in m^2 s^{-1}; π is the main component of phase α; used in multicomponent models, Eq. [1], [2], [4], and [6]
$\lambda_{eff} = \lambda_{dry} + \sqrt{S_w}\left(\lambda_{wet} - \lambda_{dry}\right)$ $\lambda_{wet} = \lambda_s^{1-\phi}\lambda_w^\phi$ $\lambda_{dry} = \lambda_s^{1-\phi}\lambda_n^\phi$	[17]	effective thermal conductivity coefficient in W m^{-1} K^{-1} (Somerton et al., 1974); used in non-isothermal models, Eq. [7]

Non-isothermal Multiphase Multi-component Processes in Porous Media

We consider the entire vadose zone including root systems to be a non-isothermal, multiphase, multicomponent system. In most natural systems, roots will grow in the unsaturated zone. The unsaturated soil, excluding roots, can be described as a two-(fluid)-phase, multicomponent, non-isothermal porous media system, with water and air as the two partly miscible fluid phases. In this study, we neglect mechanical deformation of the solid soil matrix. The governing equations of such a system are given by the conservation equations for mass, momentum, and energy (see Eq. [1], [2], and [7] in Table 2). Choosing the primary variables wetting-phase pressure p_w and non-wetting-phase saturation S_n, the subsequent assumptions and constitutive relations are necessary to close the system.

We assume local thermodynamic equilibrium (e.g., Class et al., 2002). This means that the temperature is the same in all phases, the capillary pressure will be a function of only the saturation, and the chemical activity of all components is locally equal in all phases. We compute the phase composition by means of Raoult's and Henry's law, Eq. [11] and [12]. To this end, we postulate the restriction that the mole fractions of all components in a phase add up to 1 (see Eq. [13]). Because there is no void space, the saturations have to add up to 1 (see Eq. [14]). Heat conduction is described with an effective thermal conductivity λ_{eff}, Eq. [17], depending on the local volume fractions and the thermal conductivities of all fluid phases and the solid phase. All phases can store energy. The diffusive component fluxes within a phase are described by Fick's law, with effective diffusion

coefficients depending on porosity, saturation, and tortuosity of the porous structure (see Eq. [16]). Moreover, constitutive models relating capillary pressure $p_c = p_n - p_w$ and relative permeability $k_{r\alpha}$ to water saturation S_w are necessary (see Eq. [8] and [9]). In this work, a van Genuchten type model (van Genuchten, 1980) is used. Note that the modular DuMu^x material framework also offers other pre-implemented choices like Brooks–Corey type models (Brooks and Corey, 1964).

Fluid properties, such as dynamic viscosity, density, and binary diffusion coefficients are functions of pressure and temperature. The pressure dependence of the water density may be non-negligible under conditions of very high negative pressures (Davitt et al., 2010), depending on the application. However, under such conditions it is generally questionable whether the presented theory holds. Gray and Hassanizadeh (1991) discussed the theory's paradoxes—in particular, the questionable assumption that at zero flow velocity, the water phase will exhibit a hydrostatic pressure distribution—and the very high negative water pressures often accepted at low water saturations. Nevertheless, it is still the most commonly applied theory for flow in the unsaturated zone. For more information on modeling multiphase flow in porous media, see Helmig (1997).

Modeling Processes in the Vadose Zone

The following sections describe in detail which model assumptions are sensible to formulate consistent mathematical models and coupling conditions for the various processes occurring in the vadose zone, focusing on the processes depicted in Fig. 1.

Flow and Transport in Unsaturated Soil

As described above, the unsaturated soil can be described as a two-(fluid)-phase, multicomponent, non-isothermal porous media system (see Eq. [1] and [2]). Below, we discuss possible simplifications of the model and their limitations.

Often, we can exploit the fact that the viscosity of air μ_n is much smaller than the viscosity of water. Therefore, air can be assumed infinitely mobile, with the mobility of air $\Lambda_n = k_{rn}/\mu_n \rightarrow \infty$ in comparison to the mobility of water Λ_w. In that case, the conservation equations need to be computed only for the water phase. Note that as a consequence, the pressure of air inside the soil pores is constant and equivalent to the atmospheric pressure. The resulting water mass balance, Eq. [3], still contains the influence of air in the storage term and the constitutive relationship for the relative permeability k_{rw} (see Eq. [9]). Assuming incompressibility of water (ρ_w = constant) and constant water viscosity μ_w, this model is known as the Richards equation (Richards, 1931). We will, however, more generally assume that density and viscosity are functions of pressure and temperature. Note that in soil science, the Richards equation is usually formulated using the water content θ, which can be easily transformed into the water saturation S_w by multiplication with the soil porosity ϕ_s, $\theta := \phi_s S_w$.

The Richards equation is the most commonly applied model in the unsaturated zone. However, the model's applicability is limited if one of the assumptions is violated or the application has a focus on air flow, e.g., volatile components transported in air (Szymkiewicz, 2013). For example, when soil dries by evaporation, water vapor transport in the pore space is particularly important as soon as a dry zone is established inside the porous medium. Szymkiewicz (2013) listed several cases where the Richards equation inaccurately describes the problem, even when the focus is on water flow. The mobility ratio Λ_n/Λ_w can become small for small air saturation as the relative permeability k_{rn} decreases, while k_{rw} is high. This violates the Richards assumption of infinite mobility and introduces significant errors (Forsyth, 1988). Szymkiewicz (2013) mentions that the Richards equation produces insufficient results if obstacles (e.g., highly water saturated layer) hinder the air contact with the atmosphere. All three cases readily occur in applications with plants in the vadose zone. We consider a detailed analysis on the limitations of the Richards equation beyond the scope of this work. However, we provide the necessary tools and modeling to tackle unsaturated flow problems according to the individual requirement of the application and provide an example to support this claim below.

We can describe the transport of components other than the main components (water and air) in the soil by additional advection–diffusion–reaction equations (see, e.g., Eq. [4]). For the simplified, Richards-type model, it is then assumed that the component exists only in the water phase. Note that the dissolved component might influence fluid properties like water density and viscosity in addition to pressure and temperature. For more complex applications, DuMu^x contains specialized soil flow models than can replace the two-phase flow model, such as soil flow models including biomineralization (Hommel et al., 2015), salt precipitation (Jambhekar et al., 2016), or miscible three-phase flow for soil remediation applications in the vadose zone (Class and Helmig, 2002).

Regarding the discretization of the soil domain, to our knowledge, all currently available computational soil–root models use structured Cartesian grids. We have no such technical restriction and can describe irregularly shaped geometries like plant pots (see example below) and layered and fractured soil domains with unstructured or locally refined grids (see example below).

Root Xylem Flow and Transport

Inside the plant roots, water flows through the root xylem, a bundle of tubes composed of cell walls. The driving force for xylem flow is the pressure gradient caused by the transpiration in the stomata of the leaves (cohesion–tension theory [Tyree, 1997]).

The single-phase flow in each tube can be described by Poiseuille's law. Averaging leads to a Darcy's law analogy for the model equations, where the axial conductivity K_{ax} and the pressure gradient in the xylem is used to describe the one-dimensional flow (Doussan et al., 1998). The mass balance equation for sap flow in the xylem, Eq. [5], is also referred to as the single-phase

flow equation in a rigid porous medium or bundle-of-tubes model. The axial root conductivity is a parameter gained from measurements and changes with root age (Steudle and Peterson, 1998), root radius (Vercambre et al., 2002), or environmental conditions (Lovisolo and Schubert, 1998).

The transport of, for example, minerals in the xylem sap can be modeled by one or more additional advection–diffusion–reactions (see Eq. [6]). A one-dimensional advection–diffusion–reaction equation can be derived by integrating the three-dimensional equations over a cross-section of a segment.

To the end of modeling a hierarchical network of root segments, the segment equations have to be coupled at branching points by appropriate coupling conditions. We enforce continuity of pressure and mole fractions at the junctions. For the advective term, we use a first-order upwind scheme generalized for bifurcation as described by Sandve et al. (2012).

Root Water Uptake

At the soil–root interface, water and solutes are exchanged between the root system and the embedding soil. Water flow from soil into the root is mainly driven by pressure differences between the soil close to the root and the pressure inside the roots (Steudle and Peterson, 1998) and can be described by

$$\hat{q}_{\text{uptake}} = 2\pi R k_{\text{rw}} K_{\text{rad}} \left(\overline{p}_{\text{s}} - p_{\text{r}} \right) \rho_{\text{w}} \qquad [18]$$

where K_{rad} is the radial conductivity, an effective parameter including effects of all possible transport paths through outer root layers to the xylem tubes, and $\overline{p}_{\text{s}}$ and p_{r} are the water pressures in the surrounding soil and the xylem, respectively. As addition to Steudle and Peterson (1998), we introduce k_{rw}, the previously described dimensionless relative permeability, to account for the reduction in water mobility in the drying soil around the root. When the residual saturation S_{wr} of the soil around the root is reached, the relative permeability tends to zero, with the effect that the root segment at this location cannot take up water anymore. However, note that this affects only the locality of the water uptake in our model. The full physiological response to drought and the resulting reduction in the transpiration rate, hydraulic conductivities in stem and leaves, and wilting (Bartlett et al., 2016) are beyond the scope of this work.

Integrating $\hat{q}_{\text{uptake}}$ over the length of a root segment with length l yields the net uptake flux $Q_{\text{uptake}} = \int_0^l \hat{q} \, d\zeta$. In a coupled soil–root model, $\overline{p}_{\text{s}} = \overline{p}_{\text{s}}(\zeta)$ is the average soil pressure on the surface, computed as the mean pressure on a circle with radius R (the root segment radius) at each integration point (cf. D'Angelo and Quarteroni, 2008):

$$\overline{p}_{\text{s}} = \frac{1}{2\pi R} \int_0^{2\pi} p_{\text{s}} R \, d\theta \qquad [19]$$

Note that simply evaluating the soil pressure at the root segment centerline is mathematically not defined because the soil pressure solution is singular at that point. Moreover, it is physically sensible that the water uptake depends on the pressure at

the soil–root interface. The averaging operator, Eq. [19], occurs naturally when deriving the reduced network model (D'Angelo and Quarteroni, 2008).

If component transport is considered, e.g., to describe the root uptake of nutrients, salts, pesticides, or fertilizers, the uptake mechanisms are specific to the considered solute molecule. Here, concentration gradients, solubility, and plant type influence the transfer. Varying demand for nutrients by the plant alters active uptake rates. Solute uptake maybe described by Michaelis–Menten-type descriptions for active uptake or passive models like an advection–diffusion model for solutes transported with the water.

If non-isothermal processes are important, for example, when considering evaporation, an additional energy conservation equation (see Eq. [7]) needs to be solved in the root and the soil domains. This leads to additional but analogous coupling terms describing conduction and convection at the soil–root interface.

The uptake model enters the equations of both systems, xylem flow and soil flow, as a source–sink term. The source of one subsystem depends on the difference between the water pressures in both subsystems. Let Ω denote the soil domain, Λ the root domain, and $\Gamma = \Omega \cap \Lambda$ their interface. For the soil system, inserting the source term in Eq. [16] yields

$$\frac{\partial \left(\phi_{\text{s}} S_{\text{w}} \rho_{\text{w}} \right)}{\partial t} - \nabla \cdot \left[\rho_{\text{w}} \frac{k_{\text{rw}}}{\mu_{\text{w}}} \mathbf{K} \left(\nabla p_{\text{w}} + \rho_{\text{w}} g \nabla z \right) \right] = $$
$$-2\pi R K_{\text{rad}} k_{\text{rw}} \left(\overline{p}_{\text{s}} - p_{\text{r}} \right) \delta_{\Gamma} \qquad \text{in } \Omega \qquad [20]$$

while the root system equation becomes

$$\pi R^2 \frac{\partial \left(\phi_{\text{r}} \rho_{\text{w}} \right)}{\partial t} - \nabla \cdot \left[\rho_{\text{w}} K_{\text{ax}} \left(\frac{\partial p_{\text{w}}}{\partial \zeta} + \rho_{\text{w}} g \frac{\partial z}{\partial \zeta} \right) \right] = $$
$$2\pi R K_{\text{rad}} k_{\text{rw}} \left(\overline{p}_{\text{s}} - p_{\text{r}} \right) \qquad \text{in } \Lambda \qquad [21]$$

The delta distribution δ_{Γ} in Eq. [20] restricts the source term q to the soil–root interface:

$$\int_{\Omega} \hat{q} \delta_{\Gamma} dx = \int_{\Gamma} \hat{q} d\zeta \qquad [22]$$

hence it has units of m^{-2} and the property $\int_{\Omega} \delta_{\Gamma} dx = 1$.

During the daytime, the pressure difference between the soil and the root system, $\overline{p}_{\text{s}} - p_{\text{r}}$, is usually positive, resulting in a positive source at the root subsystem and a negative source (sink) at the soil subsystem. In this case, water is transferred from the soil into the root. During nighttime or during water scarcity the flux can also be locally negative. The root gives back water to the soil in what is known as *hydraulic redistribution* (often also *hydraulic lift* but redistribution can be observed in any direction) (Richards and Caldwell, 1987; Smart et al., 2005). Hydraulic redistribution is a phenomenon seen in many different plant species and regions. More information on the topic can be found in Caldwell et al. (1998), Caldwell and Richards (1989), Neumann and Cardon (2012), and Manoli et al. (2017).

Transpiration

Transpiration occurs due to the difference in vapor pressure in the stomata of the leaves and the atmosphere and is the driving force in root water uptake and sap flow (cohesion–tension theory). Rates depend on wind speed and the temperature of the atmosphere as well as net radiation receipt by the leaves, which triggers stomata opening to take up CO_2 (Bierhuizen and Slatyer, 1965; Jarvis and McNaughton, 1986) and increases water losses due to evaporation. During nighttime, the stomata usually close, which leads to a decline in transpiration, although nighttime transpiration has been observed in several species and can be up to 10% of daytime transpiration (Snyder et al., 2003).

Transpiration rates are typically imposed as Neumann boundary conditions at the root collar (Javaux et al., 2008). It is possible to simulate diurnal variations of the transpiration rate as a time-dependent Neumann boundary condition. In experimental setups, transpiration rates can often be measured. As noted by Javaux et al. (2008), such imposed flux conditions can lead to water stress, when the plant is not able to extract enough water from the soil to meet the transpirational demand. Following Javaux et al. (2008), we switch to a Dirichlet condition enforcing the permanent wilting point pressure ($p_w = -1.5$ MPa) after this pressure is reached at the root collar. This boundary condition assumes that the root collar pressure is kept constant by the stomatal response of the plant to water stress. The transpiration rate subsequently decreases. We switch back to prescribing a transpiration rate if the transpiration rate predicted with the Dirichlet boundary condition would exceed the transpiration rate predicted by the usual diurnal cycle (see below).

For growing root systems, we follow Clausnitzer and Hopmans (1994) and estimate the transpiration rate as a function of the root volume, V_{root}, with the following ratios:

$$\rho_{root} = \frac{m_{root}}{V_{root}}, \quad \varphi_{r:s} = \frac{m_{root}}{m_{shoot}}, \quad \varphi_{A_L:s} = \frac{A_L}{m_{shoot}}, \quad \varphi_{r_T:A_L} = \frac{r_T}{A_L} \quad [23]$$

where ρ_{root} is the root (mass) density; $\varphi_{r:s}$ is the ratio between the root biomass, m_{root} (below the surface) and the shoot biomass, m_{shoot} (above the surface); $\varphi_{A_L:s}$ is the ratio between leaf area, A_L, and the shoot biomass; and $_{r_T} A_L$ is the ratio between the transpiration rate, r_T, and the leaf area. These ratios are generally varying with time and environmental factors. However, for the sake of simplicity, we here assume constant ratios (see below).

Root Growth

For applications like evaluating agricultural irrigation plans or soil stabilization by plant roots, it is important to focus closely on water management in the soil during plant growth, i.e., when the plant's root system grows. Root growth depends on soil properties (Hewitt, 2004; Jakobsen and Dexter, 1987; Dunbabin et al., 2011) and root water uptake on the root architecture (Tron et al., 2015; Lynch, 1995). Models of root growth, with explicit description of the root system architecture, coupled with root water uptake and subsurface nutrient transport processes are important to analyze the interaction of the evolving root system with the embedding soil.

The root growth model is based on a recent C++ implementation of the RootBox algorithm (Leitner et al., 2010; Leitner and Schnepf, 2016; Schnepf et al., 2018), an algorithm based on a recursively applied branch growth procedure (see L-systems, e.g., Prusinkiewicz, 2004). The root extends at a certain growth rate. The direction has a random component emulating a finite number of possibilities for growth paths in the porous soil. It is further determined by a tropism, an active direction decision by the plant. Tropisms usually result from external stimuli like gravity (gravitropism), soil water content (hydrotropism), or the plant's tendency to continue growing in an already established direction (exotropism). When reaching a certain length, root branches create daughter branches, and the same growth procedure is applied to those branches. The algorithm results in a hierarchical tree structure and can mimic the growth of different plant species. To this end, all parameters assigned to branches are stochastically distributed parameters following experimental observations.

While not all features of RootBox are available in the current implementation, we improved several aspects concerning the numerical properties of the soil–root coupling. The aspect of local mass conservation is usually overlooked in the current root growth literature. In addition to locally mass conservative discretization methods for the governing equations, growing root systems introduce mass into the system. On the one hand, this is the biomass of a new root segment that reduces the soil pore space, effectively reducing the soil porosity, ϕ_s in Eq. [3]. Due to the discrete description of the root network, the volume fraction taken up by the root segments contained in a discrete soil cell can be easily computed by dividing the root volume in that cell by the cell volume. On the other hand, new pore space gets created in the form of the root xylem that needs to be filled with water. This is accounted for in the xylem flow balance's storage term. Looking at Reynold's transport theorem for the change of water mass in the root, $m_{w,root}$,

$$\frac{dm_{w,root}}{dt} = \frac{\partial}{\partial t} \int_{V(t)} \phi_r \rho_w \, dV + \int_{\partial V(t)} \rho_w \left(\mathbf{v}_r \cdot \mathbf{n} \right) dA \quad [24]$$

for a growing control volume $V(t)$, e.g., at the root tip, where $\mathbf{v}_r$ denotes the fluid velocity relative to the moving control volume boundary $\partial V(t)$, we see that the storage integral is not constant with time. Assuming that a newly growing root segment is instantaneously filled with water during growth, we can replace the relative velocity on the root segment boundary with the fluid velocity $\mathbf{v}_r \approx \mathbf{v}$. Using an implicit Euler time discretization to approximate the time derivative yields

$$\frac{\partial}{\partial t} \int_{V(t)} \phi_r \rho_\alpha \, dV \approx \frac{(V\phi_r\rho_\alpha)_{k+1} - (V\phi_r\rho_\alpha)_k}{t_{k+1} - t_k} \quad [25]$$

i.e., the control volume size V has to be evaluated at the next (t_{k+1}) and current (t_k) time discretization point, effectively increasing the storage term by a contribution from the volume change.

Another improvement concerns continuous growth and tiny elements occurring during growth that can cause ill-conditioned linear systems. For large time steps, the algorithm already controls the proper discretization of the created root segments and branches by a maximum segment length. However, because the branching point positions are determined by a dice roll at the creation of the branch, respecting those positions can lead to tiny elements. For small time steps, the RootBox algorithm ignores tiny segments, thus leading to discontinuous growth with time, i.e., the branch would not grow in one time step and then, for example, grow twice as much in the following time step. We avoid these small elements by allowing the vertex of the existing element at the root tip to move to increase the segment length instead of creating a new small segment. This leads to a better distribution of element sizes, with small elements occurring only at the tip of a growing branch. Moreover, this allows segments to continuously grow and thus avoids additional mass balance errors that destabilize the numerical scheme. Similar considerations have been made in the latest version of CRootBox (Schnepf et al., 2018).

Evaporation from Soil

Evaporation is a process driven by the difference in water vapor pressure in the soil and the atmosphere and therefore needs to be described by a non-isothermal, multiphase, multicomponent model. Using the standard Richards model, it is not possible to describe evaporation consistently because vapor transport is not accounted for. It is possible to adapt the Richards equation, with the additional assumption that the air-phase velocities are zero, to account for additional diffusive vapor transport in the air phase (Vanderborght et al., 2017). However, we will focus on the description of evaporation using a full two-phase, two-component model where vapor transport is inherently considered and does not require additional model constraints. Consistent approaches to model soil evaporation are, to our knowledge, mostly neglected in state-of-the-art root architecture models, although soil evaporation plays a crucial role in soil–root–atmosphere interactions.

Evaporation can be divided into two distinct stages. In the atmosphere-driven Stage I, the liquid water phase is continuously connected to the soil surface, where water evaporates at the interface with the atmosphere. Stage II evaporation begins with the successive disconnection of the liquid water phase from the surface. The evaporation front sinks into the porous soil medium and the evaporation rate is limited by vapor diffusion in the porous medium, resulting in much lower evaporation rates than in Stage I. This phenomenon has been described in various studies, e.g., Scherer (1990) and Lehmann et al. (2008).

There are different approaches to model interactions between free flow and porous medium flow. One approach is to use a two-domain model with a sharp interface separating the domains (Vanderborght et al., 2017; Mosthaf et al., 2011; Fetzer et al., 2016). The two domains are coupled at the interface. Coupling conditions need to be formulated for the balance of mass, momentum, and

energy. A simplified version is described here, where no free flow equation system is explicitly solved.

Turbulent free flow leads to the formation of a viscous sublayer, referred to as a boundary layer. Assuming that the evaporation rate is mainly influenced by water vapor diffusion through that boundary layer (Haghighi et al., 2013), the coupling conditions can be simplified by not considering momentum transfer between the porous medium and the free flow domain. Moreover, heat conduction is assumed to dominate the energy transfer, simplifying the energy balance (Fetzer et al., 2016). Assuming that the boundary layer mole fraction of water vapor in the gas phase, $x_\mathrm{n}^{\mathrm{H_2O,BL}}$, the boundary layer thickness, δ_{BL}, and the boundary layer temperature, T^{BL}, are constant, the evaporation model reduces to a Robin-type boundary condition for the soil domain. The evaporation rate driven by diffusion is calculated as in Mosthaf et al. (2014) and Fetzer et al. (2016). The mass flux of the water component at the interface can be computed as

$$f^{\mathrm{H_2O}} = D_\mathrm{n}^{\mathrm{H_2O}} \rho_\mathrm{n} M^{\mathrm{H_2O}} \frac{x_\mathrm{n}^{\mathrm{H_2O,BL}} - x_\mathrm{n}^{\mathrm{H_2O,\Gamma}}}{\delta_{\mathrm{BL}}} \qquad [26]$$

with $x_\mathrm{n}^{\mathrm{H_2O,\Gamma}}$ denoting the mole fraction of the water component in the gas phase at the interface (here, the top of the soil), and $D_\mathrm{n}^{\mathrm{H_2O}}$ being the binary diffusion coefficient of water in the gas phase.

When assuming chemical equilibrium, the mole fraction of water in the gas phase can be computed using Raoult's law (Eq. [11]). However, it is known that for very dry soil and thus high capillary pressure, stronger adhesion of water to the solid matrix reduces evaporation and shifts the liquid–vapor equilibrium in favor of the liquid phase. This relationship between the capillary pressure and the water vapor pressure $p_\mathrm{n}^{\mathrm{H_2O}}$ can be expressed by the Kelvin equation (Edlefsen and Anderson, 1943):

$$p_\mathrm{n}^{\mathrm{H_2O}} = p_{\mathrm{sat}}^{\mathrm{H_2O}} \exp\left(-\frac{p_\mathrm{c} M^{\mathrm{H_2O}}}{\rho_\mathrm{w} \mathcal{R} T}\right) \qquad [27]$$

where $p_{\mathrm{sat}}^{\mathrm{H_2O}}$ is the saturation vapor pressure of water depending on the temperature T, $M^{\mathrm{H_2O}}$ is the molar mass of water, and $\mathcal{R}$ is the universal gas constant.

The heat flux, f^{h}, due to heat conduction driven by the temperature differences of the soil surface and the boundary layer are accounted for by Fourier's law inside the boundary layer:

$$f^{\mathrm{h}} = \lambda_\mathrm{n} \frac{T^{\mathrm{BL}} - T^{\Gamma}}{\delta_{\mathrm{BL}}} \qquad [28]$$

where λ_n denotes the thermal conductivity of the non-wetting gas phase, and T^{Γ} is the soil surface temperature. The boundary layer model can be extended to include velocity-dependent boundary layer thickness or surface roughness. For further information on the theory of boundary layers and evaporation processes, see Fetzer et al. (2017) and Vanderborght et al. (2017). Several boundary layer models as well as sharp interface models solving the Navier–Stokes

equations in the free flow have been successfully realized with DuMu^x (Mosthaf et al., 2014; Fetzer et al., 2016) but are out of the scope of this work.

Numerical Model and Discretization

The introduced soil–root models result in coupled systems of nonlinear PDEs to be solved in two domains of different dimensionality. The soil problem is posed on a three-dimensional domain, the root problem on a one-dimensional network domain embedded in the three-dimensional soil domain. Both domains are discretized independently in space. The resulting meshes are non-matching. We use a finite volume method for the space discretization resulting in a locally mass-conservative scheme. In time, we discretize using the unconditionally stable implicit Euler scheme. Consequently, a system of nonlinear equations has to be solved in each time step. We use Newton's method and numerical differentiation.

In the following, we discretize Eq. [3] and [5] as examples. The other equations are discretized analogously to numerically solve the PDE system. Let Ω and Λ denote the soil and root domains, respectively. We discretize Ω and Λ into a finite number of control volumes. The discrete soil domain, Ω_h, consists of, for example, a set of n hexahedrons, E_Ω^i, so that $\Omega_h = \bigcup_{i=1}^{n} E_\Omega^i$, and the discrete root domain of a set of m lines, E_Λ^i, so that $\Lambda_h = \bigcup_{i=1}^{m} E_\Lambda^i$. The discretization process is pictured in Fig. 2. Integrating Eq. [16] and [18] over a control volume E_Ω^i and E_Λ^i, respectively, and using the divergence theorem yields

$$\int_{E_\Omega^i} \frac{\left(\phi_s S_w \rho_w\right)_{t_{n+1}} - \left(\phi_s S_w \rho_w\right)_{t_n}}{t_{n+1} - t_n} \mathrm{d}V$$
$$- \int_{\partial E_\Omega^i} \left[\rho_w \frac{k_{rw}}{\mu_w} \mathbf{K}\left(\nabla p_s + \rho_w g \nabla z\right)\right]_{t_{n+1}} \cdot \mathbf{n}\,\mathrm{d}A = \quad [29]$$
$$\int_{E_\Omega^i \cap \Lambda_h} \hat{q}_{t_{n+1}} \,\mathrm{d}\zeta \qquad \forall E_\Omega^i$$

$$\int_{E_\Lambda^i} \frac{\left(\pi R^2 \phi_r \rho_w\right)_{t_{n+1}} - \left(\pi R^2 \phi_r \rho_w\right)_{t_n}}{t_{n+1} - t_n} \mathrm{d}\zeta$$
$$- \int_{\partial E_\Lambda^i} \left[\rho_w K_{ax}\left(\frac{\partial p_r}{\partial \zeta} + \rho_w g \frac{\partial p_r}{\partial \zeta}\right)\right]_{t_{n+1}} \cdot \mathbf{n}\,\mathrm{d}a =$$
$$\int_{E_\Lambda^i \cap \Omega_h} -\hat{q}_{t_{n+1}} \,\mathrm{d}\zeta \qquad \forall E_\Lambda^i$$

Note that the delta distribution restricts the source term integral to the intersection of E_Ω^i with Λ_h, $E_\Omega^i \cap \Lambda_h$:

$$\int_{E_\Omega^i} f \delta_{\Lambda_h} \,\mathrm{d}V = \int_{E_\Omega^i \cap \Lambda_h} f \,\mathrm{d}\zeta$$

Figure 2 (right) shows such an intersection marked in red.

Note that to compute the integrals over the exchange source term between the root and the soil domain, Eq. [18], we need to compute the actual intersection lines of all E_Ω^i with Λ_h. The integrals over each intersection are approximated by a quadrature rule. At each quadrature point, the average soil pressure is evaluated on the perimeter of the corresponding cross-section, Eq. [19]. The soil–root interface coincides with the dashed lines in Fig. 2 parallel to the root segment centerline (black lines). For the integration, the soil pressure is considered constant per soil element, and no additional interpolation is applied.

Software Concept and Implementation

In the following section we present a software concept that is tailored for the numerical models arising for plant-scale soil–root interaction processes.

DuMu^x and the DUNE Framework

Our models are implemented using the software DuMu^x—an open-source simulator for flow and transport processes in porous media (Flemisch et al., 2011; Ackermann et al., 2017). DuMu^x has been successfully applied in numerous technical,
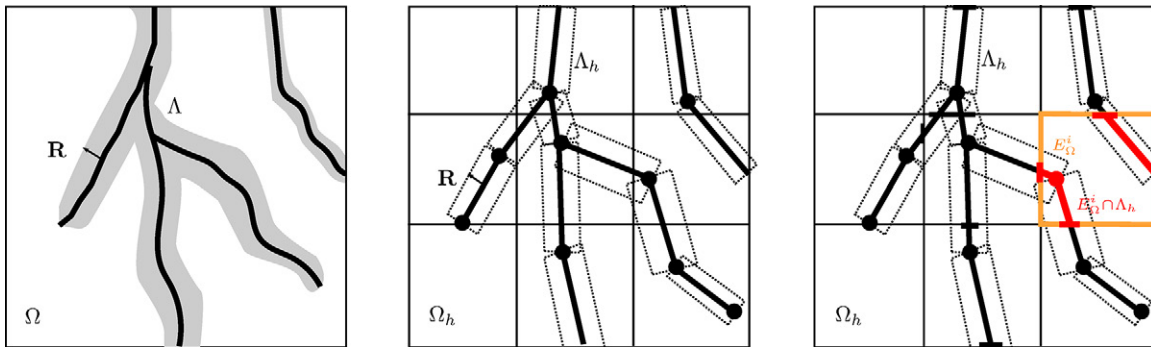

Fig. 2. Independent discretization of the two subdomains: the two continuous domains (left); both domains are discretized independently in space (middle); the resulting meshes are intersected (right), where $E_\Omega^i \cap \Lambda_h$ denotes the intersection between the soil domain element E_Ω^i and the discrete root domain Λ_h. The degrees of freedom for both subdomains, using a cell-centered finite volume scheme, are located at the centroid of the cells, where a cell in the root system is a line segment between two nodes.

biological, and hydrological applications including porous media (see the software's website at http://www.dumux.org/publications.php). DuMu^x is based on the Distributed Unified Numerics Environment (DUNE) (Bastian et al., 2008a, 2008b, 2011), an open-source scientific numerical software framework for solving PDEs. It uses modern C++ programming techniques, including templates for efficiency and general interfaces. The DUNE core modules provide an iterative solver back end (Blatt and Bastian, 2007), various grid managers, a linear algebra back end, and parallel computing features used by DuMu^x. While the idea of a plant-scale model is not new, the implementation inside a framework like DuMu^x brings several advantages and new features.

One advantage is that DuMu^x is free and open-source software, which makes the software framework sustainable and assures the quality and reproducibility of the simulation results, recently improved through the dumux-pub project (Flemisch, 2011). It facilitates and encourages each scientific publication to be accompanied by the source code necessary to reproduce the simulation results. The source code to reproduce the results of this study can be found at https://git.iws.uni-stuttgart.de/dumux-pub/Koch2017a or upon request from the authors. The software quality is another focus of DUNE and DuMu^x and is ensured through automated testing in a continuous integration work flow, recently extended by tools for system testing (Kempf and Koch, 2017).

Another advantage of using DuMu^x is the availability of many porous media models including compositional, multiphase, and non-isothermal models and a variety of constitutive laws. While most plant-scale models simulate soil water dynamics with the Richards equation only, DuMu^x is not restricted to a single soil flow model. Various available porous media models can be easily used in its place, e.g., a miscible two-phase two-component, non-isothermal model (see below), including evaporation processes. DUNE has been recently provided with the grid manager dune-foamgrid (Sander et al., 2017), specialized for one- and two-dimensional surface and network grids embedded in a world of arbitrary dimension. The grid manager was developed for, among others, applications like growing root networks.

While single plant models can usually be run on a desktop computer within minutes to hours, scenarios with multiple plants or more complex physical processes have to be run on clusters with modern parallel architectures. DUNE provides DuMu^x with the necessary parallel features (currently: distributed memory with message passing interface [MPI]). While parallel soil simulations are currently possible in DuMu^x, root system simulations are sequential

only due to dune-foamgrid not being parallel yet (Sander et al., 2017). A parallel dune-foamgrid grid manager and a suitable parallel grid coupling concept can enable fully parallel simulations in the future.

Implementation of Generalized Embedded Mixed-Dimension Models

We developed a modular software concept based on two goals: the flexible combination of existing models and constitutive laws into mixed-dimensional soil–root models, and a simple user problem setup.

DuMu^x introduces the notion of a *problem*. A problem defines a simulation scenario including domain definition and boundary and initial conditions. Traditionally, problem classes in DuMu^x also contain methods controlling simulation flow (assembly and solving). The notion of a model describes a mathematical model consisting of a system of coupled PDEs including constitutive equations needed for closure. The term *discretization* refers to the spatial and temporal discretization scheme to solve the model equation systems numerically. Each problem has an associated model and a discretization method that can be easily changed through a traits class. This means that changing, for example, from a Richards model to a two-phase model requires changing one line of C++ code for the model and a few lines for adapting the boundary and initial conditions (two equations instead of one).

Embedded mixed-dimensional problems are meta problems, problems that couple two regular problems: a bulk problem and an embedded problem. The sub-problems have their own domain, initial and boundary conditions, model, and discretization method. The meta problem controls the simulation flow and delegates single tasks to the sub-problems. The coupling, in terms of domain intersection and coupling conditions, is delegated to an implementation class that we call the *coupling manager*. The relations are depicted in Fig. 3.

Customized coupling managers can be used to implement a large variety of coupling schemes. We provide an implementation for embedded mixed-dimensional problems as described here. Tasks of the coupling manager include the computation of grid intersections to compute the coupling integrals and find the degrees of freedom of the sub-problem having dependence on the degrees of freedom of the other sub-problem. The intersections are computed using efficient algorithms based on axis-aligned bounding box volume hierarchy data structures (Ericson, 2004). Furthermore, the coupling manager transfers data between sub-problems. For example, to compute a coupling source term, Eq. [18], a root problem needs information about the soil water pressure.
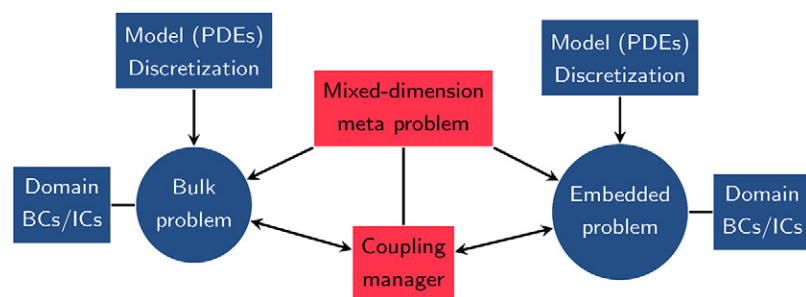
Fig. 3. Schematic of the implementation concept. The mixed-dimension meta problem combines two independent sub-problems to which it delegates tasks. In the context of soil–root models, the bulk domain is the soil domain and the embedded domain is the root system; PDE is partial differential equation, BC is boundary condition, and IC is initial condition. The coupling manager computes domain intersections and transfers data between the sub-problems on request.

Because the meta problem controls simulation flow, it can choose different solver strategies to achieve the coupling. Recall that the PDE system to be solved is nonlinear. Using Newton's method requires solving a linear system in each Newton iteration. If the equation systems are weakly coupled, an iterative procedure can be chosen to solve the linear system, where the sub-problems are solved sequentially until convergence. On the other hand, strongly coupled equation systems can be assembled into a single system matrix and solved monolithically. To this end, we assemble the linear system in the form

$$\begin{bmatrix} \mathbf{B} & \mathbf{C}_{be} \\ \mathbf{C}_{eb} & \mathbf{E} \end{bmatrix} \begin{bmatrix} \mathbf{u}_B \\ \mathbf{u}_E \end{bmatrix} = \begin{bmatrix} \mathbf{r}_B \\ \mathbf{r}_E \end{bmatrix} \qquad [30]$$

where $\mathbf{B}$ and $\mathbf{E}$ are the Jacobians of the bulk problem and the embedded problem, respectively, and $\mathbf{C}$ is the coupling Jacobian with derivatives of bulk residuals with respect to embedded degrees of freedom ($\mathbf{C}_{be}$) and vice versa ($\mathbf{C}_{eb}$), $\mathbf{u}_B$ and $\mathbf{u}_E$ denote the solution vectors of the sub-problems, and $\mathbf{r}_B$ and $\mathbf{r}_E$ are the residuals. The linear system can be solved using appropriately preconditioned iterative linear solvers.

Numerical Examples

The following examples show some results gained with the previously described models and implementations. A hydrostatic pressure profile for the water pressure was assumed in all simulations. At the top of the soil, the air pressure was assumed to be atmospheric at 0.1 MPa. Therefore, the water pressure can be calculated over the constitutive relation for the capillary pressure with $p_c = p_n - p_w$ and the van Genuchten p_c–S_w relationship, see Eq. [8]. Initial temperatures were 20°C and assumed to be constant in isothermal calculations. The axial and radial permeability of the root were uniformly chosen as $K_{ax} = 5 \times 10^{-17}$ m^4 s^{-1} Pa^{-1} and $K_{rad} = 2 \times 10^{-13}$ m s^{-1} Pa^{-1} (Huang and Nobel, 1994). The root architecture was taken from Schröder (2013). The grid is based on the reconstruction of magnetic resonance imaging data of a 2-wk-old white lupin (*Lupinus albus* L., total root length 1.56 m).

The uptake and redistribution of a tracer is simulated with a locally refined grid, which shows the simulation of simultaneous root growth and water uptake. We show the influence of soil evaporation on soil water management in an experiment-like setup. Hydraulic uplift can be observed in the model, especially if the soil dries out inhomogeneously due to a low-permeability soil layer. Finally, we show a comparison of different soil flow models with an irrigation example. All observations shown here, and even more comprehensive data, can be reproduced using the code provided in the dumux-pub repository (see above).

Tracer Transport in the Unsaturated Zone Including Roots

The following example shows a model of tracer transport and uptake by a root system. It demonstrates that grids locally refined around the embedded root network can significantly improve computational performance while maintaining a good approximation of the numerical solution.

We simulate an experiment where heavy water is used as a marking tracer to track root water uptake. The soil water dynamics are modeled with the Richards equation and xylem flow with the bundle-of-tubes model, while transport is modeled with an additional advection–diffusion equation in soil and xylem, Eq. [4] and [6]. The heavy water tracer ($x_w^{D_2O} = 3.0 \times 10^{-7}$) is initially concentrated in a small region (yellow cells in Fig. 4 at $t = 0$) in proximity to the root system of a white lupin. As the plant transpires, the tracer gets taken up with the rest of the regular water and continues to travel within the root's xylem. A constant transpiration rate of $r_T = 2.15 \times 10^{-8}$ kg s^{-1} = 1.858 g d^{-1} is enforced at the root collar as a Neumann boundary condition. The transport involves both diffusion and advection, while isotropic dispersion due to local velocity inhomogeneities is included effectively via the diffusion coefficient.

The soil grid is locally refined around the root system, leading to better approximations of pressure and concentration gradients at the soil–root interface. We refine the soil elements that are intersected by root segments. The soil has a homogeneous porosity $\phi_s = 0.4$ and intrinsic permeability $K = 2.57 \times 10^{-12}$ m^2. The van Genuchten parameters a and n are set at 0.0003 and 2.68, respectively. Figure 4 shows the simulation results. It can be seen that the cells in the vicinity of the root system are much smaller than the cells at a distance from the root system. At the tip of the root, heavy water is taken up by the root system and transported into the root xylem. In the upper part, the heavy water molecules leave the root domain back into the soil due to a reverse concentration gradient. Figure 5 shows the accumulated tracer mass that left the domain through the root collar after a given time for different soil grids: a coarse grid with 1000 soil domain grid cells (cell size, $l_c = 1.0$ cm), a uniformly refined grid with 64,000 grid cells ($l_c = 0.25$ cm), and a grid locally refined around the root, resulting in 12,186 grid cells ($l_{c,max} = 1.0$ cm, $l_{c,min} = 0.25$ cm). While the coarse resolution introduces a large error in the predicted exited mass, the locally refined grid solution is very close to the fine grid solution, with relative errors <3%. The simulation with the locally refined grid is significantly more efficient, with only a fifth of the number of unknowns. The root domain is discretized in all cases with 3476 segments ($l_{c,max} = 0.06$ cm, $l_{c,min} = 0.02$ cm). Refining the root domain grid (6952 segments, $l_{c,max} = 0.03$ cm, $l_{c,min} = 0.01$ cm) did not change the result significantly (<0.1% difference to the curves in Fig. 5 measured in relative l_2-norm). The maximum global mass conservation error with respect to the initial tracer mass in the system, 1.087 μg, is <1.0 × 10^{-9} μg in all simulations.

Water Uptake of a Growing Root System

This short example shows two growing root systems in a plant pot, using the model described above for root growth. The coupling is locally mass conservative considering the pore space created by the growing root in the root domain and the corresponding pore
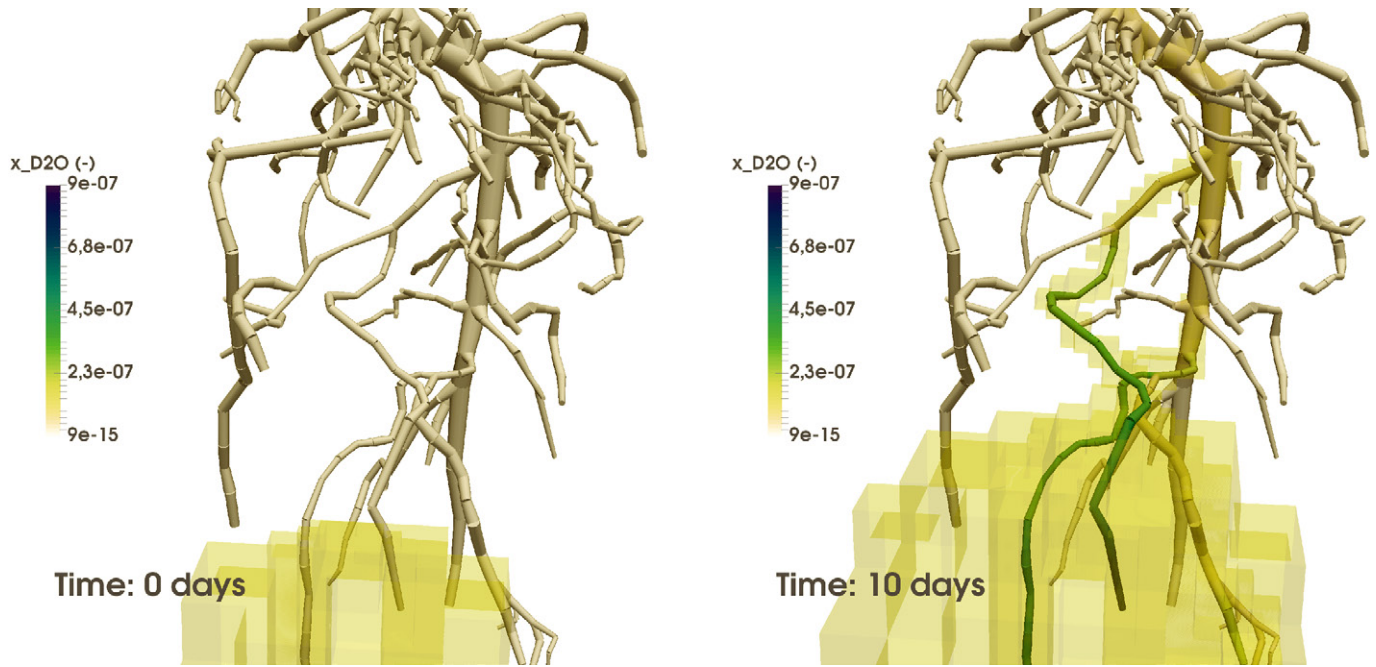
Fig. 4. Visualization of root water uptake of a heavy water tracer. The color bar represents the mole fraction of D_2O in the xylem sap. All soil cells exceeding a mole fraction of 2.0×10^{-8} are shaded. The domain is box shaped $[-0.05, 0.05] \times [-0.05, 0.05] \times [-0.1, 0.0]$ m.

space reduction in the soil. The growth is continuous with time. Small segments are avoided by moving vertices. To capture the geometry of the pot, we used an unstructured hexahedral grid for the soil domain. For simplicity, any kind of competition between the two plants, e.g., for space, water, or sunlight, is neglected.

We describe soil water dynamics with the Richards equation, Eq. [3], and root xylem flow with a bundle-of-tubes model, Eq. [5]. The initial pressure profile is hydrostatic, with a fixed water

saturation of $S_w = 0.3$ at the soil surface. The plant pot's walls are modeled as no-flow boundaries. We neglect soil evaporation and diurnal changes of the boundary conditions for simplicity. The tap root initially consists of a single segment of length $L = 1$ mm without daughter branches. The growth is parameterized using stochastic parameters fit to a white lupin according to Leitner et al. (2014).

The root system is grown at the beginning of each time step. In this example, the growth is not dependent on soil parameters
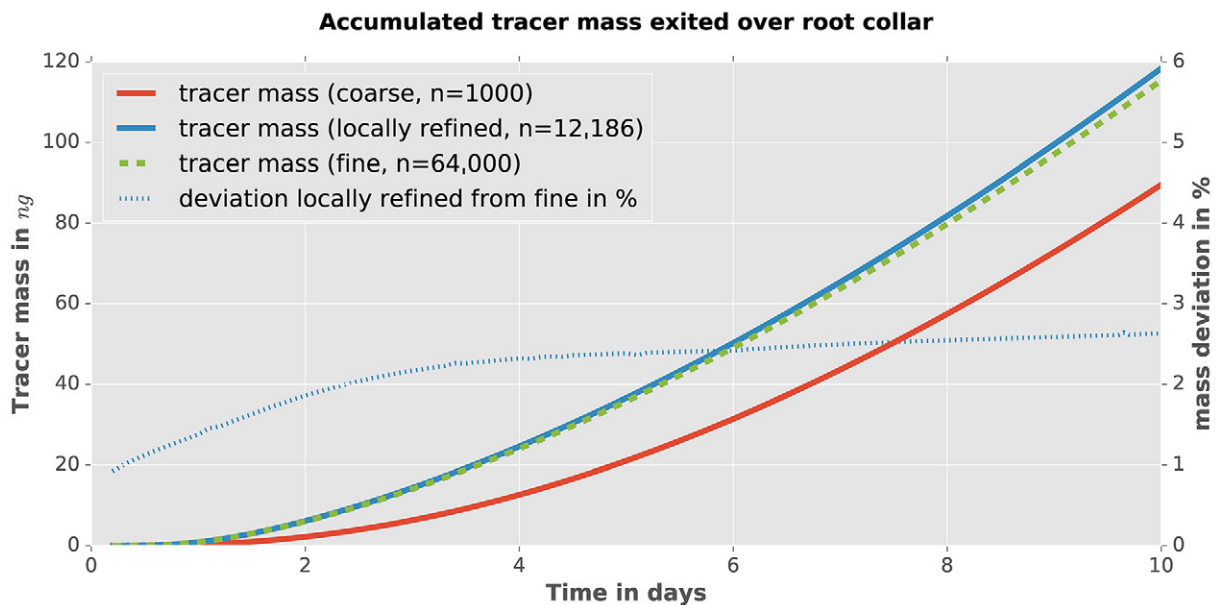

Fig. 5. Deviation of the tracer mass that left the subsurface domain through the root for a coarse grid (1000 soil domain grid cells, wall-clock time ≈3 min), a uniformly refined grid (64,000 soil cells, wall-clock time ≈30 min), and a grid locally refined around the root system and the initial heavy water reservoir (12,186 soil cells, wall-clock time ≈6 min). All computations were done on a laptop (Lenovo ThinkPad T450s, 2.3-GHz, Intel Core i5-5300U).

because we want to focus on the feature of mass conservation. In case the Newton method fails to converge in 10 steps, the time step size is cut in half. In this case, the root system is first reset to the last time step and then regrown for the smaller time step.

At the root collar, we prescribe the transpiration rate r_T as a Neumann boundary condition. We recompute the transpiration rate as a function of the root volume, V_{root}, after every growth step using

$$r_T = \frac{\rho_{root} V_{root}}{\varphi_{r:s}} \varphi_{A_L:s} \varphi_{r_T:A_L}$$

with the ratios introduced above. We chose $\rho_{root} = 750$ kg m^{-3}, $\varphi_{r:s} = 0.5$, $\varphi_{A_L:s} = 20$ m^2 kg^{-1}, $\varphi_{r_T:A_L} = 2.78 \times 10^{-8}$ m^3 s^{-1} m^{-2}; see Clausnitzer and Hopmans (1994) for comparable values. For instance, for a root mass of 10 g, this results in a maximum transpiration rate of 1 g d^{-1}. Figure 6 shows the resulting root architecture at $t_1 = 49$ h and $t_2 = 119$ h, together with the soil water saturation. It can be seen on the right and the bottom of the plant pot that the root system respects the domain boundaries.

Errors in the water mass balance stayed within the range of the numerical precision ($\approx 1.0 \times 10^{-12}$ g d^{-1}). The mass balance error, if it is not considered that growing roots have to be filled with water, is on average 0.015 g d^{-1} on the first day and rises to 0.075 g d^{-1} at the end of 1 wk. To better understand the magnitude of the error, we computed it as a percentage of the transpiration rate, an indicator of the magnitude of the mass flow rates of interest. The error is 17 and 2% of the average transpiration rate on the first day and at the end of 1 wk, respectively. Recall that the transpiration rate in this example is a function of root volume, while the error depends on the newly created root tip volume and the growth rate.

Evaporation from Soil and Root Water Uptake

The last example demonstrates the complex interactions that can be captured with the model applied to a scenario with plant transpiration and evaporation from the soil.

Evaporation dries the soil and is a fundamental process in every bare natural soil. To see the influence of evaporation on soil water management, we define three scenarios. Two scenarios show natural evaporation from a bare soil, where Case A features an embedded root system and Case B does not. In the third scenario (Case C), the soil surface is sealed, hence it is showing plant transpiration without the effect of evaporation from the soil. All scenarios feature soil in an acrylic box under realistic environmental conditions. The box has a cubic shape with a side length of $a = 10$ cm. During the simulation, there is no irrigation. Key driving processes are thus the plant's transpiration and evaporation processes drying the soil.

The soil has an initial saturation of $S_w = 0.99$ and a temperature of $T = 275.15$ K. It is then placed in a wind tunnel with perfectly controlled atmospheric conditions such that the evaporated water is immediately transported away from the plant and the soil and the water vapor mass fraction above the soil stays constant at $X_{ref} = 0.008$, corresponding to a relative humidity of 55% at 20°C. The atmospheric temperature is varied sinusoidally between 10°C at night and 20°C during the day to simulate night–day cycles. The air is flowing over the box that is open on the top for the bare soil scenario, with a stable boundary layer of thickness $\delta_{BL} = 0.0016$ m. The local influence of the plant's stem and leaves on the atmospheric flow and the boundary layer are neglected. The acrylic box has a thermal conductivity of $\lambda_{pg} = 0.184$ W m^{-1} K^{-1}, a homogeneous thickness of $d_{pg} = 0.005$ m, and exchanges energy with the atmosphere and the soil system through heat conduction. Values for the thermal conductivity $\lambda_r = 0.5$ W m^{-1} K^{-1} and
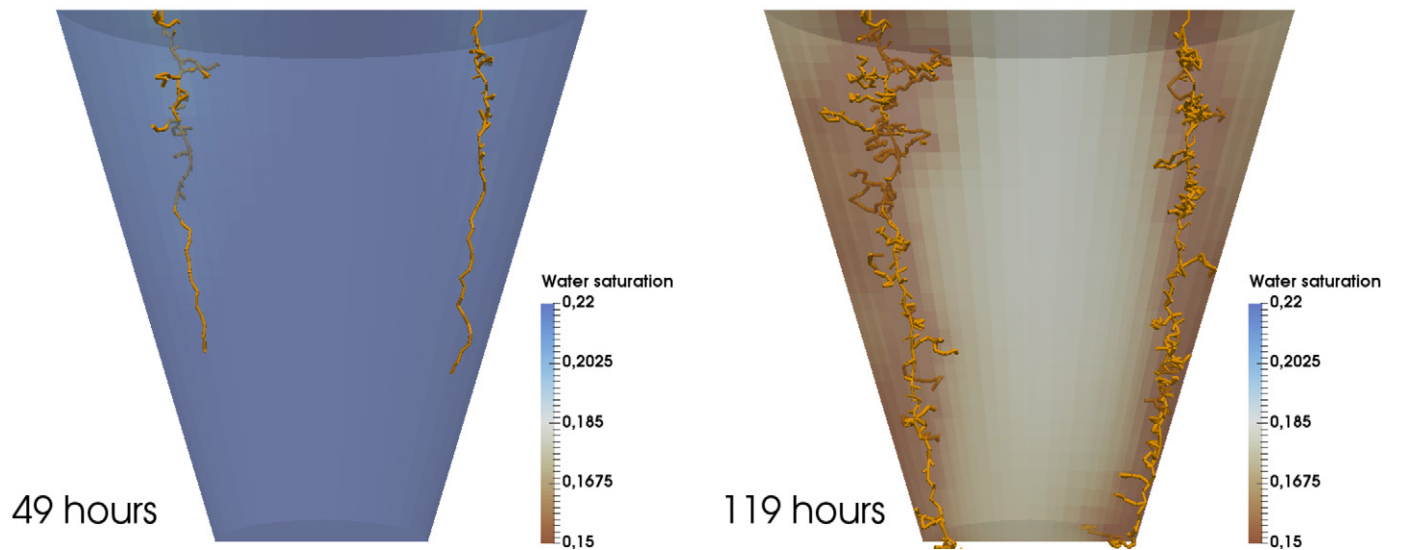

Fig. 6. Root water uptake of two growing root systems driven by transpiration at the plants' leaves as a function of the respective root volume, $r_T = r_T(V_{root})$, with a locally mass conservative coupling scheme. Vertical cut through a plant pot with the shape of a truncated cone. The root segments are visualized as tubes scaled with the segment radius. The soil color visualizes the water saturation. The domain is 10 cm high, with an upper radius of 5 cm and a lower radius of 2 cm (12,150 grid cells).

heat capacity $c_{s,r}$ = 1637 J kg^{-1} K^{-1} of the roots were taken from Jayalakshmy and Philip (2010).

In the middle of the acrylic box, a thin soil layer with a much lower permeability and lower porosity divides the soil domain into a lower half and an upper half. The layer blocks water flow from the lower to the upper compartment. Thus, water passing the layer is forced through the root xylem. Spatial parameters and the position of the layer can be seen in Fig. 7. To describe the fluid mechanical processes in the soil accurately, we use the miscible two-phase, two-component non-isothermal porous medium model, Eq. [1], [2], and [7], described above. The root xylem flow by a non-isothermal bundle-of-tubes model, Eq. [5] and [7].

At the root collar, a sinusoidal transpiration rate with a peak of r_T = 2.314 × 10^{-7} kg s^{-1} (20 cm^3 d^{-1}, assuming ρ_w = 1.0 g cm^3) is prescribed, simulating night–day cycles. This accumulates to 10 cm^3 d^{-1}.

Figure 8 shows the evaporation rates and transpiration rates simulated during a week for the three test cases. On the top, the evaporation rates with (Case A, red line) and without plant (Case B, blue line) are plotted. The solid red line shows the total evapotranspiration rate, i.e., soil evaporation and plant transpiration. The transition to the Stage II evaporation regime, driven by water vapor diffusion in the gas phase (Lehmann et al., 2008), is clearly visible starting on the first day. Stage II evaporation with the root starts earlier due to the additional drying effect by the transpiring plant. Note, however, that the effect of the plant above the surface on the flow in the wind tunnel is neglected in the model. Leaves throw shadows on the soil, and transpiration at the stomata would cool down the atmospheric air, leading to an even more reduced evaporation rate. It can be seen that during Stage I evaporation is the dominant effect for water transport to the atmosphere, whereas during Stage II transpiration exceeds evaporation during the daytime. First, the roots take up water from deeper soil layers where water is still available, while evaporation is limited to the top layer of the soil, which is already dry. Second, the vapor transport through the dry porous medium is slow and diffusion driven, whereas the transport of water through the root xylem is driven by advection and is thus faster.

Figure 8 (bottom) shows transpiration rates for the case with evaporation (Case A) compared with the scenario with a sealed soil surface (Case C). Recall that we switch to a Dirichlet boundary condition when the plant is under water stress (p_w = −1.5 MPa at the root collar), hence the transpiration rate decreases significantly. It is obvious that evaporation will lead to water stress occurring much earlier. Without soil evaporation, the maximum transpiration rate can be kept up throughout the simulation. For the test case including evaporation, the permanent wilting point pressure at the root collar is reached after 4 d and transpiration rates start to decrease. When potential transpiration rates drop during the night, then the maximum transpiration occurs at higher pressures again. However, with growing transpiration rates during the day, the plant is under stress conditions again, at an even earlier time than the day before. Note that the complex physiological reaction of the plant to drought cannot be captured by the presented model.
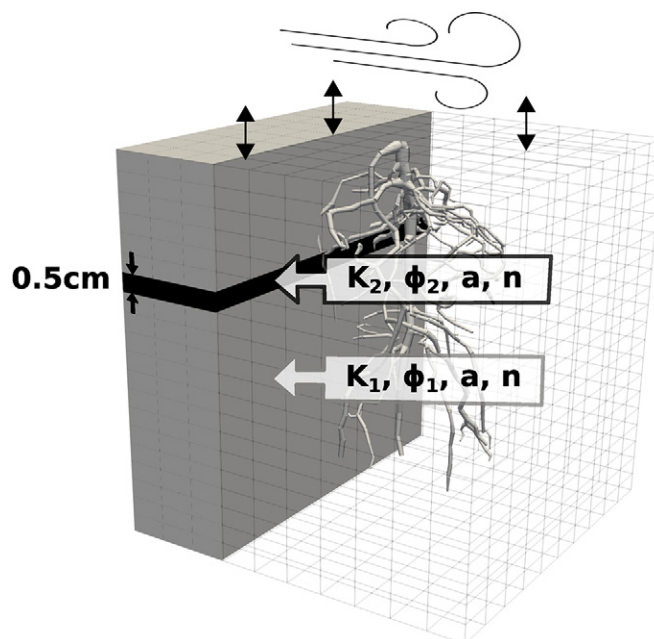

Fig. 7. A root system embedded in a cubic acrylic box ($[-0.05, 0.05]$ × $[-0.05, 0.05]$ × $[-0.1, 0.0]$ m) filled with soil in contact with the free flow in the wind tunnel, the upper and lower parts of the soil are separated by a low permeability layer (black); the soil parameters are K_1 = 2.57 × 10^{-12} m^2, K_2 = 2.57 × 10^{-15} m^2, ϕ_1 = 0.3, ϕ_2 = 0.01, van Genuchten parameters a = 5.8 × 10^{-4} Pa^{-1}, n = 17.8.

The simulation provides only an estimate when wilting or other reactions to drought can be expected.

Figure 9 shows the three-dimensional water distribution in the soil box. Evaporation dries out the soil predominantly at the soil surface. At night, an additional effect of the root on the water distribution in the soil can be observed. The figure shows the source terms of the root and saturation in the soil in the beginning of the simulation, after t = 1.5 d, and at t = 4 d at night for the scenario with bare soil. During the night, as the transpiration rates are smaller and the pressure in the root rises and is higher than in the surrounding soil in the upper soil layer, leading to exudation of water into the soil, while in the lower soil layer, water enters the root. This hydraulic lift through the root system cannot be seen in the scenario without evaporation (not depicted in Fig. 9) because the soil dries out more or less evenly in all soil layers by root water uptake, whereas evaporation only dries out the upper soil layer due to the low permeability layer in the middle of the box. The effect of evaporation on local root water uptake can also be seen in the result after 1.5 d during the day, where root water uptake happens only in the lower soil layers, which are still saturated. This supports the proposition that soil evaporation has a major influence on the locality of water distribution, root water uptake, and hydraulic redistribution in the vadose zone.

Water Irrigation and Different Models for Flow in Unsaturated Soil

Finally, we model an irrigation event and demonstrate how the model can be used to analyze the limitations of the assumptions
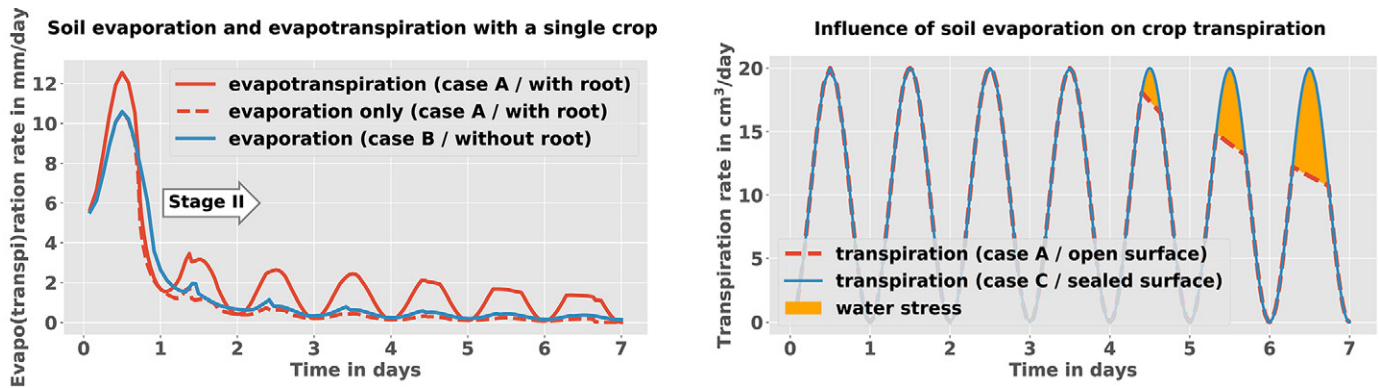
Fig. 8. Evaporation and evapotranspiration rates for Cases A and B (top), and transpiration rates for Cases A and C, i.e., with and without the influence of evaporation from the soil (bottom).

made to derive the Richards equation. In a setting such as given above, we look at an acrylic box filled with homogeneous soil and containing the same white lupin root system. Without loss of generality of our results, we assume isothermal processes. The soil water pressure initially follows a hydrostatic pressure distribution with water saturation at the top at $S_{\text{w,top}} = 0.3$. The soil is heavily irrigated for 5 min, modeled by fixing the top pressure to $p_{\text{w}} = p_{\text{n}} - p_{\text{c}}(S_{\text{w}} = 0.98)$ with $p_{\text{n}} = 0.1$ MPa. Subsequently, an evaporation boundary condition, as described in the previous example, is prescribed. The boundary conditions for the irrigation episode are chosen to demonstrate the largest difference between the Richards soil flow model, Eq. [3], and the two-phase two-component soil flow model, Eq. [1] and [2], whereas the evaporation episode is expected to be described well by both models.

While the Dirichlet boundary conditions for the irrigation episode show the difference between the models well, they may be hard to realize in an experiment. Neumann boundary conditions, prescribing an influx, model a flow-controlled pump. In a second numerical irrigation experiment, we inject 187 g of water during 5 min at a constant flow rate, resulting in the same injected water mass as with Dirichlet boundary conditions, for the two-phase, two-component model.

Prescribing Neumann boundary conditions fixes the flow rate, independent of the resistance of the air phase. The infiltrating water decreases the effective soil permeability for the air phase, hindering the air from leaving the soil domain. However, because air has to leave the domain at the soil surface to allow more water to infiltrate, water accumulates in the upper part of the soil. Once the soil close to the soil surface is fully saturated, the air phase is completely trapped. Still, the boundary condition enforces the same flow rate, which leads to compression of the air phase and consequently to a large pressure increase. This is not expected from an irrigation experiment with a free surface. Using the two-phase two-component model, a third type of boundary condition can be realized. In a third numerical irrigation experiment, we artificially extend the box domain at the soil surface by 5 mm. Although the domain extension is not a porous medium, we use the same equations as in the soil domain to approximate a free surface. We assign a value of $\phi_{\text{s}} = 1.0$ to the

porosity, use a high intrinsic permeability value to minimize the flow resistance, and neglect capillary pressure, $p_{\text{c}} = p_{\text{n}} - p_{\text{w}} = 0$. At the top of the domain extension, the air pressure is fixed at $p_{\text{n}} = 0.1$ MPa, the water saturation at $S_{\text{w}} = 0$, and the mass fraction of water in the air phase at $X_{\text{n}}^{\text{H}_2\text{O}} = 0.008$. On the sides, the domain extension is closed (no-flow Neumann boundary conditions). We inject 187 g of water during 5 min at a constant flow rate through a source term in the first cell layer of the domain extension (right above the soil surface). The domain extension creates a reservoir that allows the water to pond on the soil surface.

Figure 10 shows the total water mass for the first numerical experiment (Dirichlet boundary conditions) in the soil box with time. Clearly, under the condition of heavy irrigation, the Richards assumptions are violated. Due to high water saturation at the soil surface, the air mobility becomes very low, while the water mobility is at its maximum. This leads to an overestimation of the infiltration velocity when using the Richards equation because the effect of the additional resistance caused by the trapped air on the water flow is neglected. The overestimation of the air-phase mobility results in a mass overhead of the total water mass in the soil box of approximately 20% after 5 min for the Richards model. In the subsequent evaporation period, in which the evaporation rate is constant due to a high availability of water, constant atmospheric conditions, and the assumption of an isothermal process, both models predict the same evaporation rates.

For the second experiment (Neumann boundary conditions), the upper part of the soil domain is increasingly saturated. After 2.5 min, the saturation is so high, and thus the air mobility so low, that the remaining air in the soil box starts to compress and the pressure starts increasing with the two-phase two-component model. After 5 min, the air pressure has risen to $p_{\text{n}} = 0.2$ MPa due to the Neumann boundary conditions, which continue to force the same constant irrigation flow rate into the domain. The Richards model, on the other hand, completely ignores the resistance that the water phase poses to the air phase and thus largely overestimates the infiltration velocity.

The unrealistic conditions at the end of the second experiment are addressed in the third experiment modeling a pseudo-free
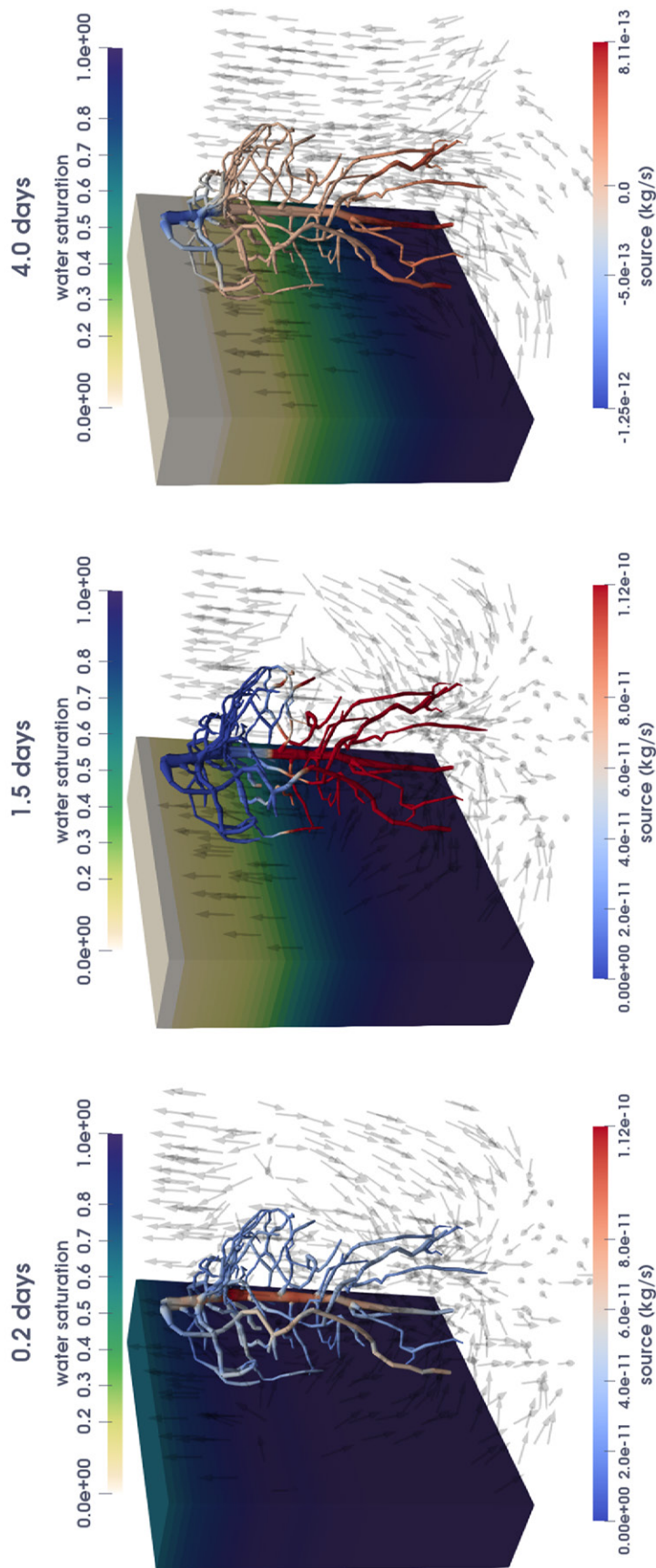
Fig. 9. Source terms and saturation at the beginning of the simulation after 1 d and in the night after 4 d. The hydraulic redistribution through the root can be seen on the upper dry soil layer as negative source terms in the root.

surface, where the water is allowed to pond at the soil surface. As shown in Fig. 11, the water infiltrates and the saturation in the upper part of the soil rises as expected until t = 220 s. Then, the first cell of the domain extension starts to fill up with water, i.e., the water starts ponding. After 5 min, the ponding water table reaches 2.5 mm, corresponding to a water pressure increase of 25 Pa at the soil surface.

Although ponding was neglected in the first experiment, the third experiment shows that the amount of water ponding at the given soil permeability and irrigation rate is rather small and results in a very small pressure increase at the soil surface. In conclusion, the boundary conditions in the first experiment are realistic enough to assess the difference between the two soil models.

Discussion and Model Limitations

A mass-conservative tracer transport model with a locally refined grid improves the approximation of gradients of tracer concentration in the vicinity of the root. Local refinement is a very simple measure to increase accuracy while maintaining computational efficiency. Refining the soil elements intersected by root segments led to significant improvement of the solution with respect to a uniformly refined solution with similar results to refinement strategies based on a priori and a posteriori error estimates (Schröder et al., 2009). Using grid refinement has the advantage that no additional assumptions about the local pressure function, such as cylindrical symmetry for analytical solutions (Schneider et al., 2010), have to be imposed. Although not presented here, local refinement can be done adaptively in each time step when dealing with more complex propagation patterns. Mass conservation is an essential property when analyzing tracer substance transport such as for minerals, nutrients, or contaminants. For the transport of nutrients, the model currently includes only transport in the soil domain, uptake, and passive transport in the root xylem. However, nutrient transport can be more complicated, involving active transport and bidirectional transport in the root phloem. Additionally, the model is currently disconnected from the total carbon balance of the plant, involving also above-surface processes like photosynthesis and stem and leaf growth.

We have presented a root architecture model coupled with root water uptake, and we argued that growth models need to describe continuously growing root systems when coupling with hydro-mechanical processes in the embedding soil to ensure mass

conservation. We have shown that the root xylem volume created by growing roots has to be considered to obtain a locally and globally mass conservative scheme; otherwise the global mass balance error was reported to be more than 2% of the transpiration rate for the presented example. The applied fully implicit coupling scheme has the advantage of no time step restriction regarding numerical stability. Therefore, the new scheme is capable of modeling the strongly coupled processes on relevant time scales with reasonable computational effort. Note that the growth model, in its current state, does not include dependence on soil properties like permeability, porosity, and water saturation. However, such model extensions are anticipated in the model design so that models available in the literature can be incorporated. The effects of competition of plants for water, nutrients, or sunlight are not part of the current model. Again, growth is also influenced by above-surface processes that are out of the scope of the model presented here.

Introducing a boundary layer soil evaporation model as a complex boundary condition for the soil surface allows a consistent description of evapotranspiration and the investigation of hydraulic redistribution. We show that evaporation and transpiration mutually influence each other, and both are important processes for water transport into the atmosphere. However, evaporation is particularly important in the well-saturated Stage I evaporation regime, whereas transpiration is dominant in the water vapor diffusion-driven Stage II evaporation regime. Soil evaporation rates are higher without plants, although looking at accumulated evapotranspiration rates in dry or plant-covered soils, plant transpiration plays a major role in water transfer to the atmosphere. The model allows analysis of every process in detail and singling out of the effect of certain processes. Such analysis is indispensable for understanding evapotranspiration in natural environments. Nonetheless, the current model concept is still limited in describing the feedback of processes above the surface,

such as shadows cast by the vegetation, and the influence of atmospheric conditions, such as the influence of wind speed on stomatal closure (Schymanski and Or, 2016).

Finally, the flexibility of the model and software concept to adapt to the required complexity, regarding the considered physical processes, is demonstrated above. The example suggests that for specific cases, a more complex model may help to analyze the simpler model's limitations.

For complex process interdependencies, it is often hard to provide analytical estimations on which to base simplifying assumptions. For such cases, it is valuable to have a framework in which single processes can be eliminated to analyze process interdependencies numerically. If a certain indicator can be identified (the total injected mass in the experiment above), it can be monitored while changing between different levels of complexity of the model. If a simplified model exhibits large errors compared with the reference solution of the most comprehensive model, the assumptions on which the simplification was based are most likely violated.

The Richards model assumptions are valid in a vast number of cases. However, there are specific processes where the Richards model needs to be extended (e.g., non-isothermal soil evaporation [Vanderborght et al., 2017]) or replaced by a more general two-phase description, in particular, for cases with high water saturation or interest in volatile components. We show one example of an irrigated system where these assumptions are not valid anymore and a more complex description of the system is necessary. Specifically, the air phase is not freely connected to the atmosphere anymore but blocked by the infiltrating water. At high water saturations, the air mobility approaches zero and violates the assumption of a high mobility ratio of the water and gas phases. The experiment above shows how we use the presented model framework to assess model limitations for a specific application case.
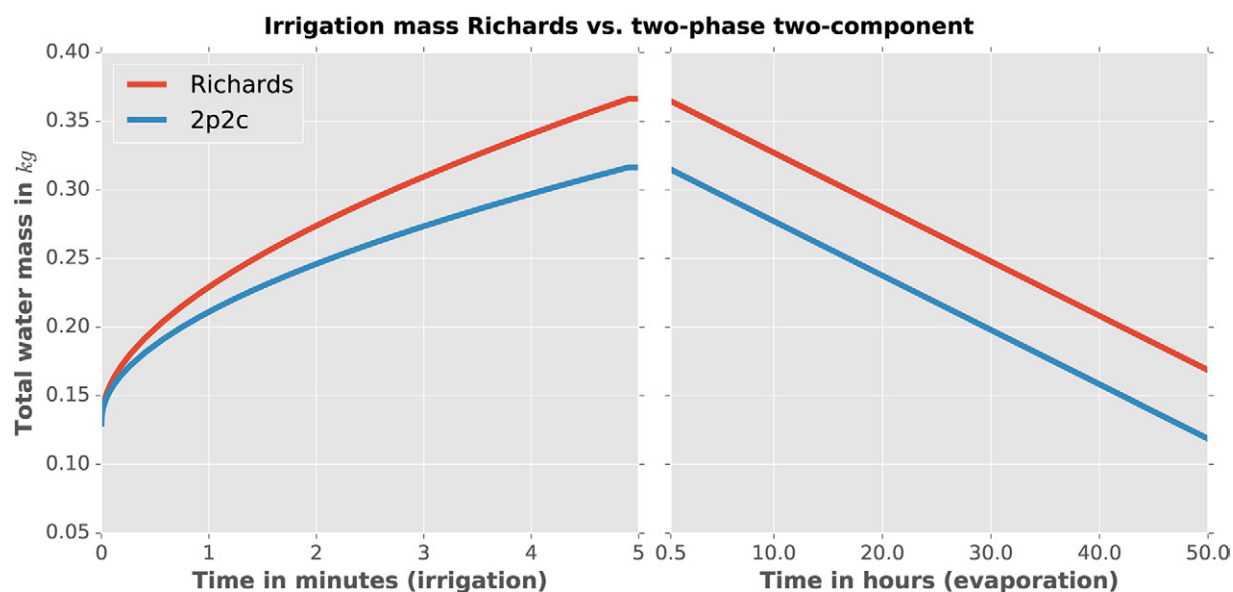

Fig. 10. Comparison of the total water mass under the influence of strong irrigation (modeled by Dirichlet boundary conditions) and evaporation from the soil in the soil box using two different soil flow models: the Richards model and the two-phase, two-component model. The soil domain is box shaped $[-0.05, 0.05] \times [-0.05, 0.05] \times [-0.1, 0.0]$ m.
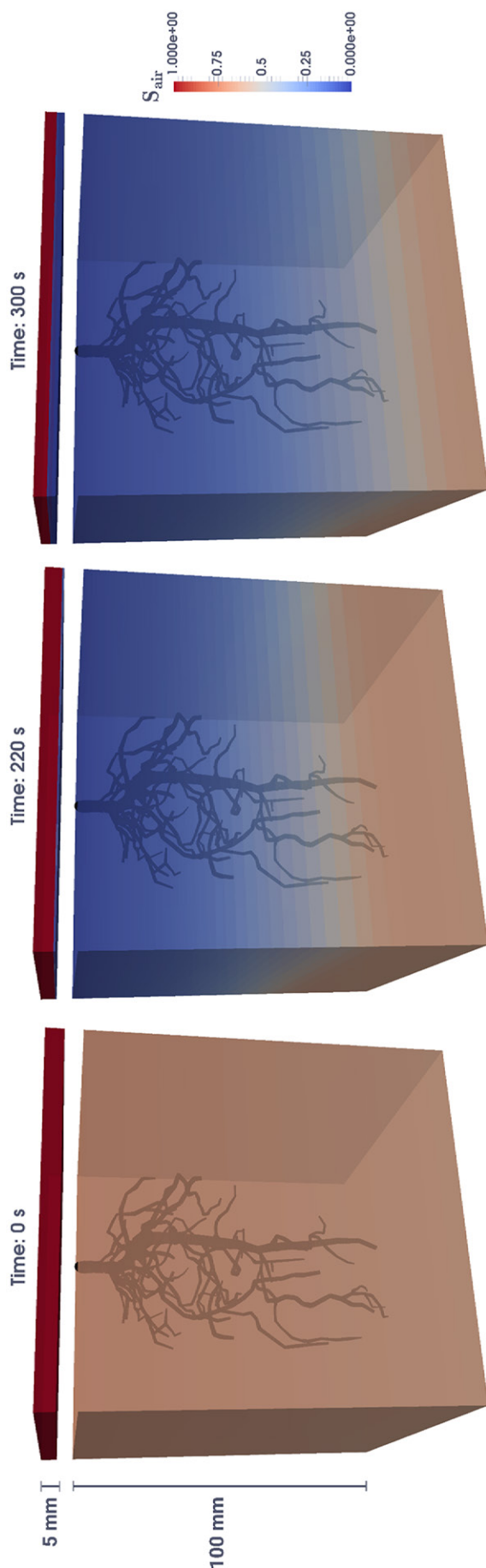
Fig. 11. Air saturation (S_{air}) at three time points for the third irrigation experiment with domain extension at the soil surface. The domain extension is shown detached from the soil domain for visualization purposes.

Summary and Outlook

We presented a simulation framework for plant-scale soil–root interaction modeling with a focus on fluid-mechanical processes. Four simulation experiments demonstrated its new features. The modular, flexible software design and the generalized model concept make it a strong tool for developing complex, nonlinear soil–root interaction models. The software is publicly available under an open-source license.

Due to its modular structure, the framework allows a quick change between different implemented model concepts. Moreover, the framework makes it simple to add transport equations or an energy equation to the system, which may be strongly coupled to the equations governing water flow. Note that exchanging soil flow models is not the only benefit of a flexible framework. By using numeric differentiation and a Newton method, arbitrarily complex nonlinear boundary conditions or source and sink terms may be implemented, parameters can nonlinearly depend on the solution, and material laws and constitutive relations can be conveniently adapted. Last but not least, the coupling conditions at the soil–root interface, being a current topic of research, are customizable. Note that most flexibility comes at a low or no additional performance cost due to the implementation at compile time with C++ templates.

We suggest that locally refined grids for soil–root models can increase computational efficiency while maintaining accuracy of the solution. The uptake model is presented in a consistent framework resulting in a convergent and locally mass-conservative numerical scheme, including evolving computational grids. We present an analysis of the competing effects of plant transpiration and evaporation from bare soil, under the limitation that the above-surface influence of the plant on the atmospheric conditions and vice versa was neglected. We showed that complex fluid-mechanical models, such as the one presented, are important to verify model assumptions for specific simulation scenarios.

The model is yet to be coupled to physiological response models and models for processes above the surface such as surface runoff, turbulent air flow, and the growth of plant stems and leaves. Such models would enable a detailed description of evapotranspiration and carbon balances. By combining established root architecture models with the presented comprehensive soil flow dynamic models, the framework is a valuable tool for analyzing root architecture dependence on water distribution and availability. The further development of the modeling framework also depends on an active community providing interesting features. Its focus on fluid mechanics, while being extensible and flexible, makes the simulation framework particularly appealing to researchers interested in the details of fluid-mechanical process interactions in coupled root–soil systems and the details of a numerical description of complex embedded mixed-dimensional processes.

References

Ackermann, S., M. Beck, B. Becker, H. Class, T. Fetzer, B. Flemisch, et al. 2017. DuMux 2.11.0. CERN, Geneva, Switzerland. doi:10.5281/zenodo.439488

Bartlett, M.K., T. Klein, S. Jansen, B. Choat, and L. Sack. 2016. The correlations and sequence of plant stomatal, hydraulic, and wilting responses to drought. Proc. Natl. Acad. Sci. 113:13098–13103. doi:10.1073/pnas.1604088113

Bastian, P., M. Blatt, A. Dedner, C. Engwer, J. Fahlke, C. Gersbacher, et al. 2011. DUNE, Distributed and unified numerics environment. Interdiscip. Ctr. for Sci. Comput., Heidelberg, Germany. http://www.dune-project.org.

Bastian, P., M. Blatt, A. Dedner, C. Engwer, R. Klöfkorn, R. Kornhuber, et al. 2008a. A generic grid interface for parallel and adaptive scientific computing: II. Implementation and tests in DUNE. Computing 82:121–138. doi:10.1007/s00607-008-0004-9

Bastian, P., M. Blatt, A. Dedner, C. Engwer, R. Klöfkorn, M. Ohlberger, and O. Sander. 2008b. A generic grid interface for parallel and adaptive scientific computing: I. Abstract framework. Computing 82:103–119. doi:10.1007/s00607-008-0003-x

Bierhuizen, J., and R. Slatyer. 1965. Effect of atmospheric concentration of water vapour and CO2 in determining transpiration–photosynthesis relationships of cotton leaves. Agric. Meteorol. 2:259–270. doi:10.1016/0002-1571(65)90012-9

Blatt, M., and P. Bastian. 2007. The iterative solver template library. In: B. Kågström et al., editors, Applied parallel computing: State of the art in scientific computing, 8th International Workshop, Revised Selected Papers, Umeå, Sweden. 18–21 June 2006. Springer, Berlin. p. 666–675. doi:10.1007/978-3-540-75755-9_82

Brooks, R.H., and A.T. Corey. 1964. Hydraulic properties of porous media and their relation to drainage design. Trans. ASAE 7:26–0028. doi:10.13031/2013.40684

Caldwell, M.M., T.E. Dawson, and J.H. Richards. 1998. Hydraulic lift: Consequences of water efflux from the roots of plants. Oecologia 113:151–161.doi:10.1007/s004420050363

Caldwell, M.M., and J.H. Richards. 1989. Hydraulic lift: Water efflux from upper roots improves effectiveness of water uptake by deep roots. Oecologia 79:1–5. doi:10.1007/BF00378231

Class, H., and R. Helmig. 2002. Numerical simulation of non-isothermal multiphase multicomponent processes in porous media: 2. Applications for the injection of steam and air. Adv. Water Resour. 25:551–564. doi:10.1016/S0309-1708(02)00015-5

Class, H., R. Helmig, and P. Bastian. 2002. Numerical simulation of non-isothermal multiphase multicomponent processes in porous media: 1. An efficient solution technique. Adv. Water Resour. 25:533–550. doi:10.1016/S0309-1708(02)00014-3

Clausnitzer, V., and J.W. Hopmans. 1994. Simultaneous modeling of transient three-dimensional root growth and soil water flow. Plant Soil 164:299–314. doi:10.1007/BF00010082.

D'Angelo, C., and A. Quarteroni. 2008. On the coupling of 1D and 3D diffusion-reaction equations: Application to tissue perfusion problems. Math. Models Methods Appl. Sci. 18:1481–1504. doi:10.1142/S0218202508003108

Davitt, K., E. Rolley, F. Caupin, A. Arvengas, and S. Balibar. 2010. Equation of state of water under negative pressure. J. Chem. Phys. 133:174507. doi:10.1063/1.3495971

Diggle, A.J. 1988. ROOTMAP: A model in three-dimensional coordinates of the growth and structure of fibrous root systems. Plant Soil 105:169–178. doi:10.1007/BF02376780

Doussan, C., L. Pagès, and G. Vercambre. 1998. Modelling of the hydraulic architecture of root systems: An integrated approach to water absorption model description. Ann. Bot. 81:213–223. doi:10.1006/anbo.1997.0540

Dunbabin, V.M., M. Airey, A. Diggle, M. Renton, Z. Rengel, R. Armstrong. 2011. Simulating the interaction between plant roots, soil water and nutrient flows, and barriers and objects in soil using rootmap. In: F. Chan et al., editors, Proceedings of the 19th International Congress on Modelling and Simulation (MODSIM2011), Perth, WA, Australia. 12–16 Dec. 2011. Modell. Simul. Soc. Aust. N.Z. p. 12–16,

Dunbabin, V.M., J.A. Postma, A. Schnepf, L. Pagès, M. Javaux, L. Wu, et al. 2013. Modelling root–soil interactions using three-dimensional models of root growth, architecture and function. Plant Soil 372:93–124. doi:10.1007/s11104-013-1769-y

Edlefsen, N.E., and A.B.C. Anderson. 1943. Thermodynamics of soil moisture. Hilgardia 15(2):31–298. doi:10.3733/hilg.v15n02p031

Ericson, C. 2004. Real-time collision detection. CRC Press, Boca Raton, FL.

Fatichi, S., C. Pappas, and V.Y. Ivanov. 2016. Modeling plant–water interactions: An ecohydrological overview from the cell to the global scale. Wiley Interdiscip. Rev.: Water 3:327–368. doi:10.1002/wat2.1125

Fetzer, T., K.M. Smits, and R. Helmig. 2016. Effect of turbulence and roughness on coupled porous-medium/free-flow exchange processes. Transp. Porous Media 114:395–424. doi:10.1007/s11242-016-0654-6

Fetzer, T., J. Vanderborght, K. Mosthaf, K.M. Smits, and R. Helmig. 2017. Heat and water transport in soils and across the soil–atmosphere interface: 2. Numerical analysis. Water Resour. Res. 53:1080–1100. doi:10.1002/2016WR019983

Flemisch, B. 2011. dumux-pub. Univ. of Stuttgart, Stuttgart, Germany. https://git.iws.uni-stuttgart.de/groups/dumux-pub.

Flemisch, B., M. Darcis, K. Erbertseder, B. Faigle, A. Lauser, K. Mosthaf, et al. 2011. DuMuˣ: DUNE for multi-{phase, component, scale, physics, …} flow and transport in porous media. Adv. Water Resour. 34:1102–1112. doi:10.1016/j.advwatres.2011.03.007

Forsyth, P.A. 1988. Comparison of the single-phase and two-phase numerical model formulation for saturated-unsaturated groundwater flow. Comput. Methods Appl. Mech. Eng. 69:243–259. doi:10.1016/0045-7825(88)90190-9

Gray, W.G., and S.M. Hassanizadeh. 1991. Paradoxes and realities in unsaturated flow theory. Water Resour. Res. 27:1847–1854. doi:10.1029/91WR01259

Haghighi, E., E. Shahraeeni, P. Lehmann, and D. Or. 2013. Evaporation rates across a convective air boundary layer are dominated by diffusion. Water Resour. Res. 49:1602–1610. doi:10.1002/wrcr.20166

Helmig, R. 1997. Multiphase flow and transport processes in the subsurface: A contribution to the modeling of hydrosystems. Springer, Berlin. doi:10.1007/978-3-642-60763-9

Hewitt, A. 2004. Soil properties for plant growth: A guide to recognising soil attributes relevant to plant growth and plant selection. Landcare Res. Sci. Ser. 26. Landcare Res., Lincoln, NZ.

Hommel, J., E. Lauchnor, A. Phillips, R. Gerlach, A.B. Cunningham, R. Helmig, et al. 2015. A revised model for microbially induced calcite precipitation: Improvements and new insights based on recent experiments. Water Resour. Res. 51:3695–3715. doi:10.1002/2014WR016503

Huang, B., and P.S. Nobel. 1994. Root hydraulic conductivity and its components, with emphasis on desert succulents. Agron. J. 86:767–774. doi:10.2134/agronj1994.00021962008600050005x

Jakobsen, B., and A. Dexter. 1987. Effect of soil structure on wheat root growth, water uptake and grain yield. a computer simulation model. Soil Tillage Res. 10:331–345. doi:10.1016/0167-1987(87)90022-5

Jambhekar, V.A., E. Mejri, N. Schröder, R. Helmig, and N. Shokri. 2016. Kinetic approach to model reactive transport and mixed salt precipitation in a coupled free-flow–porous-media system. Transp. Porous Media 114:341–369. doi:10.1007/s11242-016-0665-3

Jarvis, P., and K. McNaughton. 1986. Stomatal control of transpiration: Scaling up from leaf to region. Adv. Ecol. Res. 15:1–49. doi:10.1016/S0065-2504(08)60119-1

Javaux, M., T. Schröder, J. Vanderborght, and H. Vereecken. 2008. Use of a three-dimensional detailed modeling approach for predicting root water uptake. Vadose Zone J. 7:1079–1088. doi:10.2136/vzj2007.0115

Jayalakshmy, M.S., and J. Philip. 2010. Thermophysical properties of plant leaves and their influence on the environment temperature. Int. J. Thermophys. 31:2295–2304. doi:10.1007/s10765-010-0877-7

Kempf, D., and T. Koch. 2017. System testing in scientific numerical

software frameworks using the example of DUNE. Arch. Numer. Softw. 5:151–168. doi:10.11588/ans.2017.1.27447

Köppl, T., and B. Wohlmuth. 2014. Optimal a priori error estimates for an elliptic problem with Dirac right-hand side. SIAM J. Numer. Anal. 52:1753–1769. doi:10.1137/130927619

Lehmann, P., S. Assouline, and D. Or. 2008. Characteristic lengths affecting evaporative drying of porous media. Phys. Rev. E 77:056309. doi:10.1103/PhysRevE.77.056309

Leitner, D., B. Felderer, P. Vontobel, and A. Schnepf. 2014. Recovering root system traits using image analysis exemplified by two-dimensional neutron radiography images of lupine. Plant Physiol. 164:24–35. doi:10.1104/pp.113.227892

Leitner, D., S. Klepsch, G. Bodner, and A. Schnepf. 2010. A dynamic root system growth model based on L-Systems. Plant Soil 332:177–192. doi:10.1007/s11104-010-0284-7.

Leitner, D., and A. Schnepf. 2016. CRootBox. CERN, Geneva, Switzerland. doi:10.5281/zenodo.154017

Lovisolo, C., and A. Schubert. 1998. Effects of water stress on vessel size and xylem hydraulic conductivity in *Vitis vinifera* L. J. Exp. Bot. 49:693–700. doi:10.1093/jxb/49.321.693

Luckner, L., M.Th. van Genuchten, and D. Nielsen. 1989. A consistent set of parametric models for the two-phase flow of immiscible fluids in the subsurface. Water Resour. Res. 25:2187–2193. doi:10.1029/WR025i010p02187

Lynch, J. 1995. Root architecture and plant productivity. Plant Physiol. 109:7–13. doi:10.1104/pp.109.1.7

Lynch, J.P., K.L. Nielsen, R.D. Davis, and A.G. Jablokow. 1997. Simroot: Modelling and visualization of root systems. Plant Soil 188:139–151. doi:10.1023/A:1004276724310

Malézieux, E., Y. Crozat, C. Dupraz, M. Laurans, D. Makowski, H. Ozier-Lafontaine, et al. 2009. Mixing plant species in cropping systems: Concepts, tools and models: A review. Agron. Sustain. Dev. 29:43–62. doi:10.1051/agro:200705

Manoli, G., C.-W. Huang, S. Bonetti, J.-C. Domec, M. Marani, and G. Katul. 2017. Competition for light and water in a coupled soil–plant system. Adv. Water Resour. 108:216–230 doi:10.1016/j.advwatres.2017.08.004

Mosthaf, K., K. Baber, B. Flemisch, R. Helmig, A. Leijnse, I. Rybak, and B. Wohlmuth. 2011. A coupling concept for two-phase compositional porous-medium and single-phase compositional free flow. Water Resour. Res. 47:W10522. doi:10.1029/2011WR010685.

Mosthaf, K., R. Helmig, and D. Or. 2014. Modeling and analysis of evaporation processes from porous media on the REV scale. Water Resour. Res. 50:1059–1079. doi:10.1002/2013WR014442.

Mualem, Y. 1976. A new model for predicting the hydraulic conductivity of unsaturated porous media. Water Resour. Res. 12:513–522. doi:10.1029/WR012i003p00513.

Neumann, R.B., and Z.G. Cardon. 2012. The magnitude of hydraulic redistribution by plant roots: A review and synthesis of empirical and modeling studies. New Phytol. 194:337–352. doi:10.1111/j.1469-8137.2012.04088.x

Pagès, L., G. Vercambre, J.-L. Drouet, F. Lecompte, C. Collet, and J. Le Bot. 2004. Root Typ: A generic model to depict and analyse the root system architecture. Plant Soil 258:103–119. doi:10.1023/B:PLSO.0000016540.47134.03

Postma, J.A., C. Kuppe, M.R. Owen, N. Mellor, M. Griffiths, M.J. Bennett, et al. 2017. OpenSimRoot: Widening the scope and application of root architectural models. New Phytol. 215:1274–1286. doi:10.1111/nph.14641

Prusinkiewicz, P. 2004. Modeling plant growth and development. Curr. Opin. Plant Biol. 7:79–83. doi:10.1016/j.pbi.2003.11.007

Richards, J.H., and M.M. Caldwell. 1987. Hydraulic lift: Substantial nocturnal water transport between soil layers by *Artemisia tridentata* roots. Oecologia 73:486–489. doi:10.1007/BF00379405

Richards, L.A. 1931. Capillary conduction of liquids through porous mediums. Physics 1:318–333. doi:10.1063/1.1745010

Roose, T., and A. Schnepf. 2008. Mathematical models of plant–soil interaction. Philos. Trans. R. Soc. London, Ser. A 366:4597–4611. doi:10.1098/rsta.2008.0198

Sander, O., T. Koch, N. Schröder, and B. Flemisch. 2017. The DUNE FoamGrid implementation for surface and network grids. Arch. Numer. Softw. 5:217–244. doi:10.11588/ans.2017.1.28490

Sandve, T., I. Berre, and J. Nordbotten. 2012. An efficient multi-point flux approximation method for discrete fracture–matrix simulations. J. Comput. Phys. 231:3784–3800. doi:10.1016/j.jcp.2012.01.023

Scherer, G.W. 1990. Theory of drying. J. Am. Ceram. Soc. 73:3–14. doi:10.1111/j.1151-2916.1990.tb05082.x

Schneider, C.L., S. Attinger, J.-O. Delfs, and A. Hildebrandt. 2010. Implementing small scale processes at the soil–plant interface: The role of root architectures for calculating root water uptake profiles. Hydrol. Earth Syst. Sci. 14:279–289. doi:10.5194/hess-14-279-2010

Schnepf, A., D. Leitner, M. Landl, G. Lobet, T.H. Mai, S. Morandage, et al. 2018. CRootBox: A structural–functional modelling framework for root systems. Ann. Bot. 121:1033–1053. doi:10.1093/aob/mcx221

Schröder, N. 2013. Three-dimensional solute transport modeling in coupled soil and plant root systems. Ph.D. diss. Univ. catholique de Louvain, Louvain-La-Neuve, Belgium. http://juser.fz-juelich.de/record/151172.

Schröder, T., L. Tang, M. Javaux, J. Vanderborght, B. Körfgen, and H. Vereecken. 2009. A grid refinement approach for a three-dimensional soil–root water transfer model. Water Resour. Res. 45:W10412. doi:10.1029/2009WR007873

Schymanski, S.J., and D. Or. 2016. Wind increases leaf water use efficiency. Plant Cell Environ. 39:1448–1459. doi:10.1111/pce.12700

Shani, U., and A. Ben-Gal. 2005. Long-term response of grapevines to salinity: Osmotic effects and ion toxicity. Am. J. Enol. Vitic. 52:148–154.

Šimůnek, J., K. Huang, and M.Th. van Genuchten. 1995. The SWMS_3D code for simulating water flow and solute transport in three-dimensional variably-saturated media. Res. Rep. 139. US Salinity Lab., Riverside, CA.

Smart, D.R., E. Carlisle, M. Goebel, and B.A. Nunez. 2005. Transverse hydraulic redistribution by a grapevine. Plant Cell Environ. 28:157–166. doi:10.1111/j.1365-3040.2004.01254.x

Snyder, K.A., J.H. Richards, and L.A. Donovan. 2003. Night-time conductance in C_3 and C_4 species: Do plants lose water at night? J. Exp. Bot. 54:861–865. doi:10.1093/jxb/erg082

Somerton, W.H., J.A. Keese, and S.L. Chu. 1974. Thermal behavior of unconsolidated oil sands. Soc. Pet. Eng. J. 14:513–521. doi:10.2118/4506-PA

Somma, F., J.W. Hopmans, and V. Clausnitzer. 1998. Transient three-dimensional modeling of soil water and solute transport with simultaneous root growth, root water and nutrient uptake. Plant Soil 202:281–293. doi:10.1023/A:1004378602378

Steudle, E., and C.A. Peterson. 1998. How does water get through roots? J. Exp. Bot. 49:775–788. doi:10.1093/jxb/49.322.775

Szymkiewicz, A. 2013. Mathematical models of flow in porous media. In: Modelling water flow in unsaturated porous media. Springer, Berlin. p. 9–47. doi:10.1007/978-3-642-23559-7_2

Tron, S., G. Bodner, F. Laio, L. Ridolfi, and D. Leitner. 2015. Can diversity in root architecture explain plant water use efficiency? A modeling study. Ecol. Modell. 312:200–210. doi:10.1016/j.ecolmodel.2015.05.028

Tyree, M.T. 1997. The cohesion–tension theory of sap ascent: Current controversies. J. Exp. Bot. 48:1753–1765. doi:10.1093/jxb/48.10.1753

Vanderborght, J., T. Fetzer, K. Mosthaf, K.M. Smits, and R. Helmig. 2017. Heat and water transport in soils and across the soil–atmosphere interface: 1. Theory and different model concepts. Water Resour. Res. 53:1057–1079. doi:10.1002/2016WR019982

van Genuchten, M.Th. 1980. A closed-form equation for predicting the hydraulic conductivity of unsaturated soils. Soil Sci. Soc. Am. J. 44:892–898. doi:10.2136/sssaj1980.03615995004400050002x

Vercambre, G., C. Doussan, L. Pages, R. Habib, and A. Pierret. 2002. Influence of xylem development on axial hydraulic conductance within *Prunus* root systems. Trees 16:479–487. doi:10.1007/s00468-002-0190-6

Zarebanadkouki, M., Y.X. Kim, and A. Carminati. 2013. Where do roots take up water? Neutron radiography of water flow into the roots of transpiring plants growing in soil. New Phytol. 199:1034–1044. doi:10.1111/nph.12330